Inorganic Chemistry

Article

pubs.acs.org/IC

Synthesis and Characterization of Electroactive Ferrocene Derivatives: Ferrocenylimidazoquinazoline as a Multichannel Chemosensor Selectively for Hg^{2+} and Pb^{2+} Ions in an Aqueous Environment

Rampal Pandey, Rakesh Kumar Gupta, Mohammad Shahid, Biswajit Maiti, Arvind Misra, and Daya Shankar Pandey*

Department of Chemistry, Faculty of Science, Banaras Hindu University, Varanasi 221 005 (U.P.), India

Supporting Information

ABSTRACT: The synthesis and characterization of ferrocene (Fc) derivatives 4-[2,5-diferrocenyl-4-(4-pyridyl)imidazolidin-1-ylmethyl]pyridine (**1**), ferrocenylmethylenepyridin-3-ylmethylamine (**2**), *N*,*N*′-bis(ferrocenylmethylene)-2,4,6-trimethylbenzene-1,3-diamine (**3**), and 6-ferrocenyl-5,6-dihydro[4,5]imidazo[1,2-*c*]-quinazoline (**4**) have been described. Structures of **1**, **2**, and **4** have been determined by single-crystal X-ray diffraction analyses. At 25 °C, **1**−**3** are nonfluorescent, while **4** displays moderate fluorescence and chromogenic, fluorogenic, and electrochemical sensing selectively toward Hg^{2+} and Pb^{2+} ions. Association constants (K_a) for Hg^{2+} and Pb^{2+} have been determined by the Benesi−Hildebrand method. Job's plot analysis supported 1:1 and 1:2 stoichiometries for Hg^{2+} and Pb^{2+} ions. Cyclic voltammograms of **1**−**4** exhibited reversible waves corresponding to a ferrocene/ferrocenium couple. The wave associated with **4** (+0.0263 V) exhibited positive (ΔE_{pa} = 0.136 V) and negative (ΔE_{pa} = 0.025 V) shifts in the presence of Hg^{2+} and Pb^{2+} ions, respectively. The mode of interaction between metal ions and **4** has been supported by ^{1}H NMR spectroscopy and mass spectrometry studies and verified by theoretical studies. It presents the first report dealing with ferrocene-substituted quinazoline as a multichannel chemosensor for Hg^{2+}/Pb^{2+} ions.

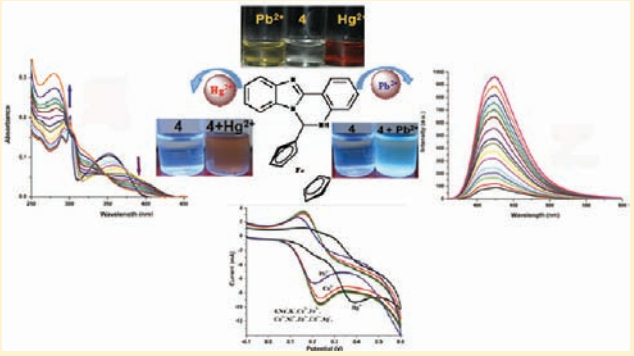

INTRODUCTION

Considerable current interest has arisen in the design, synthesis, and development of selective and sensitive methodologies for the detection of heavy- and transition-metal (HTM) ions because of their extensive use and ensuing impact on the environment.[1] Heavy-metal ions like Fe^{2+}, Zn^{2+}, Co^{2+}, Cu^{2+}, and Mn^{2+} are indispensable for biological activities; a slight disturbance in metabolic homeostasis can lead to abnormalities and fatal diseases.[2] On the other hand, HTMs like Cd^{2+}, Hg^{2+}, As^{3+}, and Pb^{2+} are known for their toxic effects, and their accumulation in human and animal bodies may lead to serious ailments.[3] Among these, mercury is considered to be extremely hazardous because its accumulation in the body causes harsh immuno/geno/neurotoxic defects.[4] The elemental or ionic forms of mercury are converted to toxic methylmercury by both bacterial and chemical actions. Its bioaccumulation within the living tissues through the food chain causes mercury poisoning and, consequently, lethal diseases.[5] Similarly, lead is a potent neurotoxin and can interfere in brain growth, nervous retardation, and triggering problems.[6] Moreover, the pollution encountered by lead is an ongoing threat to human health because it causes memory loss, mental retardation mainly in children, anemia, muscle paralysis, etc.[7] Therefore, the toxicity problems associated with Hg^{2+} and Pb^{2+} prompted chemists to develop new systems capable of their detection under aqueous conditions.[6−14] The development of fluorescent sensors for heavy-metal ions is a challenging task because most of these cause fluorescence quenching due to enhanced spin−orbital coupling and energy- or electron-transfer processes.[8] Also, the reports dealing with the detection of such metal ions under aqueous conditions or in a mixed aqueous−organic medium are rather scarce.[9]

Ferrocene and its derivatives have drawn the attention of many research groups after its discovery by Kealy and Pauson in 1951.[10] Numerous ferrocene derivatives have been prepared and characterized because of their outstanding stability, potential use in organic syntheses, homogeneous catalysis, asymmetric autocatalysis, materials science, synthesis of molecules with fascinating chirality, and redox activity.[11] Above all, ferrocene derivatives exhibit good cytotoxicity in vitro and inhibit the development of tumor in vivo.[12] In addition, C−C bonds are the backbone of many organic compounds; however, their functionality is often derived from

Received: August 2, 2011
Published: November 29, 2011

the presence of heteroatoms, which are held by C−heteroatom bonds. Although various catalytic approaches have been developed, the synthesis of organometallic compounds containing C−C bonds is still challenging.[13] In this context, ferreocene has drawn special attention because it exhibits versatile reactivity toward reactions leading to C−C bond formation.[10a,14]

Further, numerous ferrocene derivatives have already been reported as chemsensors for HTM ions.[15−17] In this regard, the application of ferrocenylquinazolines has not been investigated. With an objective of developing chemosensors based on ferrocenylquinazolines, four new compounds, **1**−**4**, have been prepared and fully characterized. It has been demonstrated that, among these, **4** serves as a multichannel (chromogenic, fluorogenic, and electrochemical) sensor for Hg^{2+}/Pb^{2+} ions. Through this contribution, we present the synthesis and characterization of **1**−**4** and single-crystal X-ray structures of **1**, **2**, and **4**. Also, we describe herein the application of **4** as a multichannel sensor for Hg^{2+}/Pb^{2+} ions.

EXPERIMENTAL SECTION

Reagents. The solvents were dried and distilled prior to use.[18] Metal nitrates viz., $NaNO_3$, KNO_3, $Ca(NO_3)_2{\cdot}4H_2O$, $Mg(NO_3)_2{\cdot}6H_2O$, $Co(NO_3)_2{\cdot}6H_2O$, $Ni(NO_3)_2{\cdot}6H_2O$, $Cu(NO_3)_2{\cdot}3H_2O$, $Zn(NO_3)_2{\cdot}6H_2O$, $Cd(NO_3)_2{\cdot}4H_2O$, $AgNO_3$, $Pb(NO_3)_2$, and $Hg(NO_3)_2$, and other common reagents and solvents were procured from SD Fine Chemicals, Ltd., Mumbai, India. Ferrocene carboxaldehyde (Fc-C), (2-aminophenyl)benzimidazole, 2,4,6-trimethylbenzene-1,3-diamine, 3-picolylamine, and 4-picolylamine were procured from Sigma Aldrich Chemical Co., Madison, WI.

General Methods. Elemental analyses for carbon, hydrogen, and nitrogen were performed on an Exeter Analytical Inc. model CE-440 CHN analyzer. IR and electronic absorption spectra were acquired on Perkin-Elmer 577 and Jasco V-670 spectrophotometers, respectively. ^{1}H (300 MHz), ^{13}C (75.45 MHz), and 2D (^{1}H−^{13}C) NMR spectra were obtained on a JEOL AL300 FT-NMR spectrometer using tetramethylsilane [$Si(CH_3)_4$] as an internal reference. Fluorescence spectra were acquired on a Varian Cary Eclipse Fluorescence spectrophotometer at room temperature. Mass spectrometry (MS) spectra (DART-MS) were recorded on a JEOL AccuTOF JMS-T100 LC mass spectrometer. Compounds **1**−**3** were dissolved in acetonitrile, while **4** was dissolved in dimethyl sulfoxide (DMSO) and dry helium (flow rate 4 LPM) used for ionization at 350 °C. Cyclic voltammetric measurements were performed on a CHI 620c electrochemical analyzer at room temperature. The experiments were performed in an airtight single-compartment cell using platinum wire as the counter electrode, glassy carbon as the working electrode, and Ag/Ag^+ as the reference electrode.

Synthesis of 4-[2,5-Diferrocenyl-4-(4-pyridyl)imidazolidin-1-ylmethyl]pyridine (1). To a stirring solution of Fc-C (0.214 g, 1.0 mmol) in benzene (10 mL) was added 4-picolylamine (0.1 mL, 1.0 mmol) dissolved in the same solvent (5 mL), and the resulting solution was heated under reflux for 24 h. After cooling to room temperature, the dark-red solution was filtered to remove any solid impurities and concentrated to half of its volume under reduced pressure. A dark-red compound separated from the filterate upon slow evaporation. It was separated by filtration, washed with diethyl ether, and dried under vacuum. Crystals suitable for single-crystal X-ray diffraction analyses were obtained by the slow diffusion of diethyl ether over a chloroform solution. Yield (0.388 g): 64%. Anal. Calcd for $C_{34}H_{32}Fe_2N_4$: C, 67.13; H, 5.30; N, 9.21. Found: C, 67.05; H, 5.19; N, 9.12. ^{1}H NMR ($CDCl_3$, 300 MHz, δ_H, ppm): 8.71 (d, J = 5.4 Hz, 2H, H-1a/H-1b), 8.46 (d, J = 5.4 Hz, 2H, H-3a/H-3b), 7.69 (d, J = 5.7 Hz, 2H, H-2a/H-2b), 7.13 (d, J = 5.7 Hz, 2H, H-4a/H-4b), 4.72 (s, 1H, H-7), 4.40 (s, 2H, H-9a/H-9d, C_5H_4), 4.36 (s, 2H, H-10a/H-10d, C_5H_4), 4.33 (s, 4H, H-9b,c/H-10b,c, C_5H_4), 4.15 (s, 5H, H-11a-e, C_5H_5), 4.12 (s, 2H, H-8), 4.09 (s, 5H, H-12a-e, C_5H_5), 3.86 (s, 1H, H-6), 3.66 (s, 1H, H-5), 2.33 (s, 1H, H-13, NH). ^{13}C{^{1}H} NMR ($CDCl_3$, 75 MHz, δ_C, ppm): 154.86, 150.5, 149.8, 149.6, 149.1, 148.8, 123.2,122.3, 87.0, 84.3, 75.5, 70.7, 69.6, 69.4, 69.0, 68.7, 68.5, 67.8, 67.6, 67.2, 66.4, 65.6, 65.3, 48.6. IR (KBr pellets, cm^{-1}): 3338 w, 1601 vs, 1571 s, 1493 m, 1362 m, 1277 m, 1189 m, 866 m, 814 s, 751 m, 478 m. DART-MS (rel intens). Calcd, found: m/z 608.1326, 609.2433 (M^+ + 1, 18%), 304.0663, 305.1139 ($M/2^+$ + 1, 100).

Synthesis of Ferrocenylmethylene-pyridin-3-ylmethylamine (2). It was prepared following the above procedure for **1** except that 3-picolylamine (1.0 equiv) was used in place of 4-picolylamine. Yield (0.213 g): 70%. Anal. Calcd for $C_{17}H_{16}FeN_2$: C, 67.13; H, 5.30; N, 9.21. Found: C, 67.02; H, 5.18; N, 9.11. ^{1}H NMR ($CDCl_3$, 300 MHz, δ_H, ppm): 8.58 (s, 1H, H-1), 8.51 (s, 1H, H-2), 8.28 (s, 1H, H-6), 7.63 (d, 1H, H-4), 7.26 (d, 1H, H-3), 4.67 (s, 4H, H-7a-d, C_5H_4), 4.39 (s, 2H, H-5), 4.17 (s, 5H, H-8a-e, C_5H_5). ^{13}C{^{1}H} NMR ($CDCl_3$, 75 MHz, δ_C, ppm): 163.1, 149.2, 148.3, 135.4, 135.1, 123.4, 80.0, 84.3, 73.2, 70.7, 69.6, 69.0, 68.6, 62.4. IR (KBr pellets, cm^{-1}): 1631 vs, 1570 m, 1471 w, 1422 m, 1248 w, 1026 m, 812 s, 713 m, 489 m. DART-MS (rel intens). Calcd, found: m/z 305.0663, 305.1139 (M^+ + 1, 100%).

Synthesis of *N*,*N*′-Bis(ferrocenylmethylene)-2,4,6-trimethylbenzene-1,3-diamine (3). 2,4,6-Trimethylbenzene-1,3-diamine (1.31 g, 1.0 mmol) dissolved in benzene (5 mL) was added to a stirring solution of Fc-C (0.215 g, 2.0 mmol) in the same solvent (10 mL), and the resulting solution was heated under reflux for 8 h. After cooling to room temperature, the reaction mixture was filtered and a dark-yellow filtrate was allowed to evaporate slowly. It afforded a yellow compound, which was separated by filtration, washed with diethyl ether, and dried under vacuum. Yield (0.326 g): 66%. Anal. Calcd for $C_{31}H_{30}Fe_2N_2$: C, 68.66; H, 5.58; N, 5.17. Found: C, 68.52; H, 5.46; N, 5.09. ^{1}H NMR ($CDCl_3$, 300 MHz, δ_H, ppm): 8.06 (s, 2H, H-2), 6. 90 (s, 1H, H-1), 4.79 (s, 4H, H-3a,d, C_5H_4), 4.48 (s, 4H, H-3b,c, C_5H_4), 4.23 (s, 10H, H-4a-e, C_5H_5), 2.15 (s, 6H, H-5a,b, CH_3), 2.03 (s, 3H, H-6, CH_3). ^{13}C{^{1}H} NMR ($CDCl_3$, 75 MHz, δ_C, ppm): 163.3, 149.9, 129.4, 121.8, 116.9, 80.8, 70.9, 69.1, 68.7, 18.1, 13.8. IR (KBr pellets, cm^{-1}): 1631 vs, 1459 w, 1224 w, 1077 m, 1030 m, 820 s, 482 s. DART-MS (rel intens). Calcd, found: m/z 543.2733, 543.2184 (M^+ + 1, 100%).

Synthesis of 6-Ferrocenyl-5,6-dihydro[4,5]imidazo[1,2-*c*]-quinazoline (4). To a stirring solution of Fc-C (1.0 mmol) in ethanol (EtOH; 15 mL) was added a solution of (2-aminophenyl)-benzimidazole (1.0 mmol) dissolved in the same solvent, and the resulting solution was allowed to heat at 60 °C for 2 h. After cooling to room temperature, the resulting solution was filtered and concentrated to half of its volume at reduced pressure. Slowly, it gave a dark-red crystalline compound, which was separated by filtration and washed with EtOH and diethyl ether. Diffraction-quality dark-red crystals were obtained by recrystallization from methanol. Yield (0.300 g): 74%. Anal. Calcd for $C_{24}H_{19}FeN_3$: C, 71.13; H, 4.73; N, 10.37. Found: C, 71.04; H, 4.62; N, 10.28. ^{1}H NMR (DMSO-d_6, 300 MHz, δ_H, ppm): 7.87 (d, J = 7.5 Hz, 1H, H-1), 7.73 (d, J = 7.5 Hz, 1H, H-4), 7.60 (d, J = 7.8 Hz, 1H, H-5), 7.32 (t, 2H, H-2, H-3), 7.29 (s, 1H, H-9), 7.22 (t, 1H, H-7), 7.08 (d, J = 8.1 Hz, 1H, H-8), 6.99 (s, 1H, H-10), 6.83 (t, 1H, H-6), 4.16 (s, 5H, H-12a-e, C_5H_5), 4.04 (s, 1H, H-11d, C_5H_4), 3.99 (s, 1H, H-11a, C_5H_4), 3.90 (s, 2H, H-11b,c, C_5H_4). ^{13}C{^{1}H} NMR ($CDCl_3$, 75 MHz, δ_C, ppm): 146.2, 143.6, 132.6, 131.6, 124.5, 122.0, 121.8, 118.5, 118.2, 114.9, 112.6, 110.6, 90.1, 68.9, 67.6, 66.7, 65.3, 63.9. IR (KBr pellets, cm^{-1}): 3384 m, 1614 vs, 1584 m, 1528 m, 1497 vs, 1446 s, 1395 s, 1320 m, 1266 s, 1320 m, 1227 m, 1153 m, 1000 w, 820 s, 748 vs, 499 m, 463 m. DART-MS (rel intens). Calcd, found: m/z 405.09284, 406.1164 (M^+ + 1, 100%).

X-ray Structure Determinations. Single-crystal X-ray data for **1** and **4** were collected on a Bruker APEX II and for **2** on a Oxford Diffraction X CALIBUR-S with Mo Kα radiation (λ = 0.710 73 Å) in a sealed tube. Structures were solved by direct methods (*SHELXS 97*) and refined by full-matrix least squares on F^2 (*SHELX 97*).[19] The non-hydrogen atoms were refined with anisotropic thermal parameters. All of the hydrogen atoms were geometrically fixed and refined using a riding model. Computer program *PLATON* was used for analyzing the interaction and stacking distances.[20] CCDC deposition numbers

dx.doi.org/10.1021/ic201663m | *Inorg. Chem.* 2012, 51, 298−311

787478 (**1**), 787479 (**2**), and 787480 (**4**) contain the supplementary crystallographic data for this paper (see also Table 1).

Table 1. Crystallographic Data of 1, 2, and 4

parameters	1	2	4
empirical formula	$C_{34}H_{32}Fe_2N_4$	$C_{17}H_{16}FeN_2$	$C_{4.17}H_{3.13}Fe_{0.17}N_{0.52}$
fw	608.34	303.18	70.31
cryst syst	monoclinic	orthorhombic	monoclinic
space group	*C*2/*c*	*Pca*21	$P2_1/n$
a (Å)	20.310(7)	18.772(4)	11.481(2)
b (Å)	9.335(3)	5.885(10)	13.352(2)
c (Å)	28.613(8)	12.489(2)	12.126(2)
β (deg)	101.138(9)	90.00	104.349(3)
volume (Å^3)	5323(3)	1379.64(4)	1801.0(5)
color and habit	red, block	red, block	red, block
Z	8	4	23
density calcd (g cm^{-3})	1.518	1.460	1.491
abs coeff (mm^{-1})	1.120	1.081	0.852
F(000)	2090	632	836
cryst size (mm^3)	0.26 × 0.24 × 0.22	0.28 × 0.23 × 0.18	0.30 × 0.28 × 0.26
θ range (deg)	2.04−28.45	3.46−24.99	2.31−28.26
reflns collected	16 985	9436	20 543
indep reflns	6568 [R_{int} = 0.1033]	2415 [R_{int} = 0.0183]	4354 [R_{int} = 0.0856]
reflns/restraint/param	4701/0/386	2349/1/ 181	4147/0/257
reflns obsd [$I > 2\sigma(I)$]	0.1661	0.0233	0.2130
GOF on F^2	1.298	0.838	1.344
final *R* [$I > 2\sigma(I)$]	R1 = 0.0691	R1 = 0.0226	R1 = 0.0803
	wR2 = 0.2262	wR2 = 0.0587	wR2 = 0.2160

Electrochemical Studies. The redox properties of **1**−**4** were followed by cyclic voltammetry in H_2O/EtOH (1:1, v/v; 100 *μ*M) containing 0.1 M [(*n*-Bu)$_4$N]ClO$_4$ as a supporting electrolyte in the potential range of +2.0 to −2.0 V at room temperature. The cyclic voltammetric experiments (metal-ion effect and titrations) were performed using a 10.0 mL solution of **4** (100 *μ*M) and 0.1 M solutions of nitrate salts of various metal ions (Li^+, Na^+, K^+, Mg^{2+}, Ca^{2+}, Fe^{2+}, Co^{2+}, Ni^{2+}, Cu^{2+}, Zn^{2+}, Cd^{2+}, Hg^{2+}, Ag^+, and Pb^{2+}). The redox potentials were referenced relative to a ferrocene/ferrocenium (Fc/Fc^+) couple as a reference (0.1 V).

UV−Vis and Fluorescence Studies. A stock solution of **4** for electronic absorption and emission studies was prepared in H_2O/EtOH (1:1, v/v; 10 *μ*M) and for various metal ions (Li^+, Na^+, K^+, Mg^{2+}, Ca^{2+}, Fe^{2+}, Co^{2+}, Ni^{2+}, Cu^{2+}, Zn^{2+}, Cd^{2+}, Hg^{2+}, Ag^+, and Pb^{2+}) by dissolving their nitrate salts in triple-distilled H_2O (10 mM). In titration experiments, a 2.0 mL solution of **4** (10 *μ*M) was taken in a quartz cuvette (3 mL; path length, 1 cm) and the solution of metal ions added gradually with the help of a micropipet. In the titration experiments, the additional interval time for each fraction of the metal ion (Hg^{2+} and Pb^{2+}) was 3 min.

Quantum-Chemical Calculations. To get information about the interaction sites of **4** containing three nitrogen atoms, quantum-chemical calculations have been performed. Among the quantum-chemical methods, density functional theory (DFT) is found to be a suitable method for our calculations.[17] All of the calculations were performed using a hybrid version of DFT and Hartree−Fock (HF) methods, namely, the B3LYP DFT method,[21a] in which the exchange energy from Becke's exchange functional[21b] is combined with the exact energy from the HF theory. Along with the component exchange and correlation functionals,[21c] three parameters define the hybrid functional, specifying how much of the exact exchange is mixed in. Although the three semiempirical parameters are optimized primarily to reproduce the thermochemistry of small organic molecules, it has been proven to perform exceptionally well for relatively larger inorganic molecules of the heteroatom. We used the 6-31G** basis set for all of the atoms except the metal atom (either Hg or Pb). For the metal atom, we used the LANL2DZ basis set with an effective-core pseudopotential.[21d−f] All of the geometry optimizations and frequency calculations (to verify a genuine minimum-energy structure) were performed using the *Gaussian 03* suite of programs.[22]

RESULTS AND DISCUSSION

The reactions of Fc-C with 3-/4-picolylamine, 2,4,6-trimethylbenzene-1,3-diamine, and (2-aminophenyl)benzimidazole were carried out in benzene/EtOH under refluxing conditions. It reacted with 4-picolylamine to afford cyclized product **1** in ∼64% yield. Characterization of **1** has been achieved by satisfactory elemental analyses and IR, ^{1}H, ^{13}C, and 2D (^{1}H−^{13}C) NMR spectroscopic and mass spectrometry (DART-MS) studies. The crystal structure of **1** was unambiguously verified by single-crystal X-ray diffraction analyses (Figure 1a). It is apparent from the crystal structure that formation of **1** takes place by condensation *cum* cyclization involving two molecules each of Fc-C and 4-picolylamine, wherein new C−C and C−N bonds are created, leading to an imidazolidine ring (Scheme 1).

The crystal structure further revealed that only one 4-picolylamine unit is involved in the cyclization process and the resulting imidazolidine ring consists of three chiral centers. 1,2-Migration of the active methylene proton from the 4-picolylamine unit to the imine nitrogen atom possibly leads to the formation of a five-membered imidazolidine ring (Scheme 2). The ^{1}H NMR spectrum of **1** displays two distinct resonances at *δ* 8.71 (*H*1a,b) and 8.46 (*H*3a,b) assignable to pyridyl and picolyl ring protons. It is noteworthy that the protons of one unit are deshielded in comparison to the other by *δ* ∼0.25. This may be attributed to the orientation of the pyridyl and picolyl rings with respect to the cyclopentadienyl (Cp) ring of the ferrocenyl moiety (Figure 2a). The H5, H6, and H7 protons of the imidazolidine ring resonated as singlet at *δ* ∼4.72−3.66 (Figure S1 in the Supporting Information, SI). The broad signal at *δ* 2.33 has been assigned to the −NH proton. Reasonably, one may think that the chiral center 2*S** has been created by C−N coupling, while 4*S** and 5*S** were created through C−C bond formation (Scheme 2). The appearance of less intense (0.25:1 ratio) doublets close to each signal attributable to the pyridyl and picolyl protons may be ascribed to the 2*R**, 4*R**, and 5*R** forms of **1** (Figure 1a). Further, to ascertain the presence of isomeric forms, the ^{1}H NMR spectrum of the single crystals were acquired and compared with that for the noncrystalline compound. Analogous spectral patterns suggested that in the solid state **1** remains in its 2*S**, 4*S**, and 5*S** forms, while it exists between two isomeric forms in the solution.

The reaction of Fc-C with 3-picolylamine was examined under analogous conditions. Surprisingly, it gave the Schiff base **2** instead of a cyclized product (Scheme 1 and Figure 1b). Its ^{1}H NMR spectrum displayed signals assignable to azomethine and methylene protons at *δ* 8.28 and 4.39 ppm along with the resonances due to other protons (Figure S2 in the SI). The presence of signals corresponding to azomethine and methylene protons suggested the formation of **2**. Notably, Fc-C reacted with 4-picolylamine to give cyclized product **1** through C−C and C−N coupling, while its reaction with 3-picolylamine afforded a Schiff base. The formation of a Schiff base over a cyclized product may be attributed to competence of the mesomeric stability of analogous picolyl carbanions through contributions from the pyridyl nitrogen atom. This is consitent with the higher stabilty of the carbanion of 4-picolylamine in comparison to 3-picolylamine.[23]

dx.doi.org/10.1021/ic201663m | *Inorg. Chem.* 2012, 51, 298−311

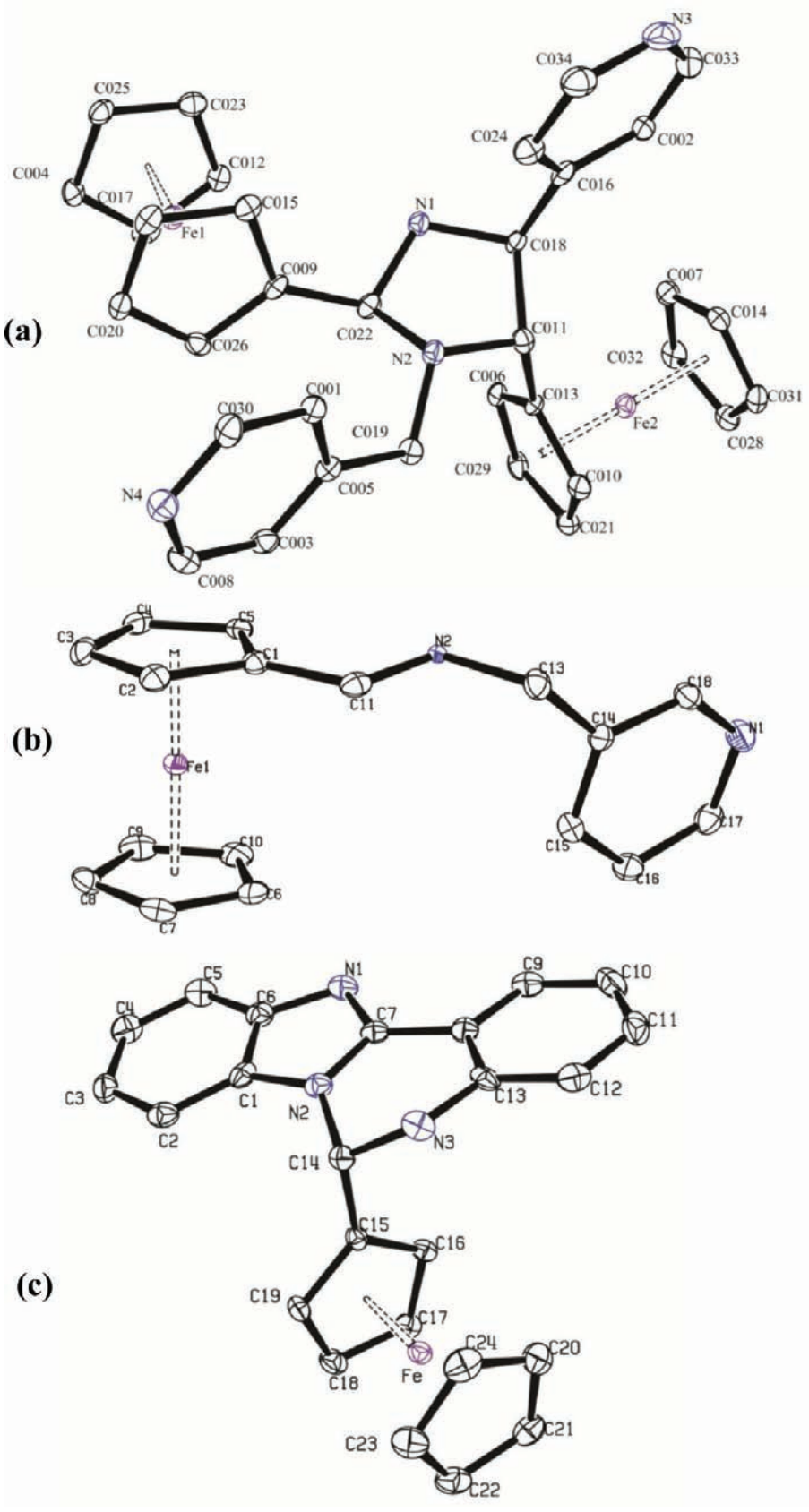

Figure 1. ORTEP views for **1** (a), **2** (b), and **4** (c) with an atom numbering scheme in 30% ellipsoid probability. Hydrogen atoms are omitted for clarity.

The reactivity of Fc-C was also examined with 2,4,6-trimethylbenzene-1,3-diamine (Scheme 1) containing two amino groups at the 1 and 3 positions. Expectedly, this gave Schiff base **3**, wherein both the amino groups of the central mesitylene ring are involved in condensation with Fc-C, which is evident from the presence of a signal due to aldimine protons

dx.doi.org/10.1021/ic201663m | *Inorg. Chem.* 2012, 51, 298–311

Scheme 1

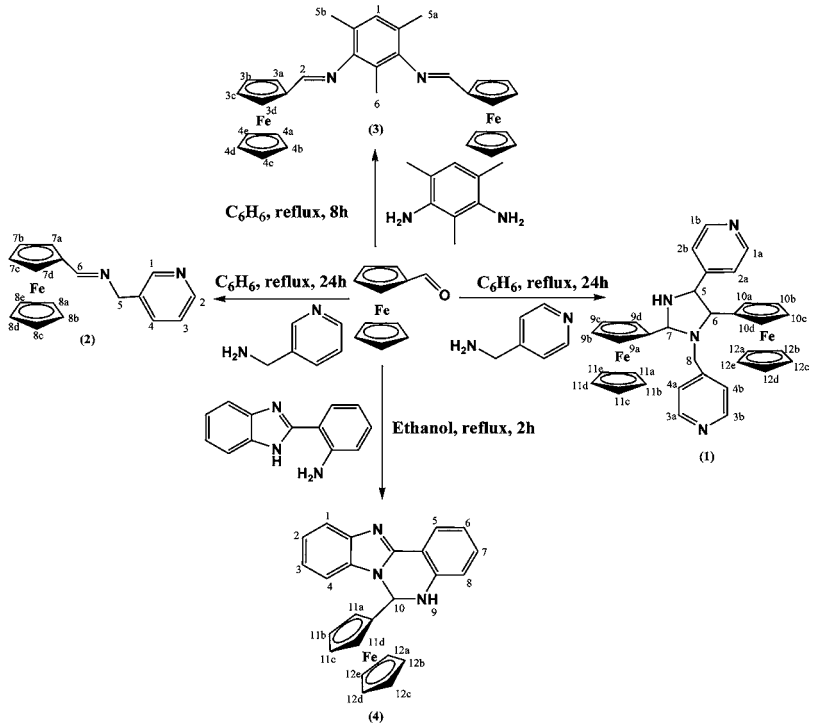

Scheme 2. Possible Route for the Formation of Imidazolidine 1

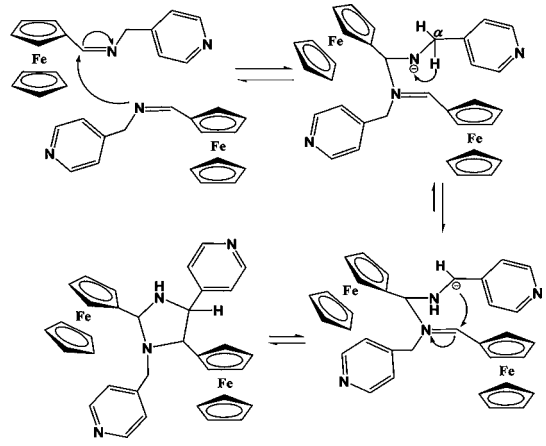

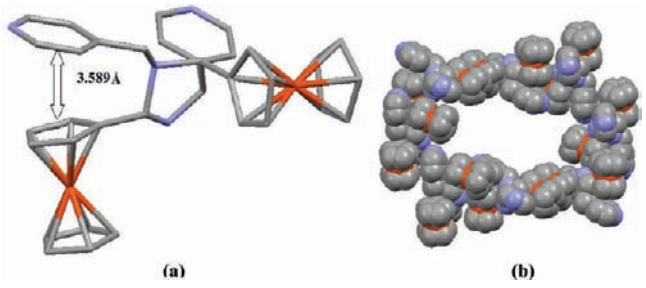

Figure 2. (a) Centroid−centroid distance between ferrocene (Fe1) and the picolyl ring in **1**. (b) Spherical view resulting from intermolecular C−H···π interactions along the crystallographic *a* axis.

at δ 8.06 ppm (Figure S3 in the SI). The reaction of Fe−C with (2-aminophenyl)benzimidazole afforded the quinazoline derivative **4** through one-pot, catalyst-free C−N coupling (Scheme 1 and Figure 1c). The ^{1}H NMR spectrum of **4** displayed singlets at δ 7.29 and 6.99 ppm, assignable to the −NH (H9) and −CH (H10) protons of the quinazoline ring (Figure S4 in the SI). The absence of a singlet above δ 8.00 ppm corresponding to the aldimine proton excludes the possibility of the formation of a Schiff base and favors C−N coupling, which has further been verified by single-crystal X-ray diffraction studies (Figure 1c).

Compounds **1**−**4** were synthesized using Fc-C as the common reactant and varying amines. Depending on the positions of the amines attached to the aromatic ring along with their functionalities, different products were expected because of the varying mesomeric stability of the carbanions associated with the respective amines. The carbanion resulting from 4-picolylamine is more stable relative to the one from 3-picolylamine, through contributions from the pyridyl nitrogen atom. Therefore, the cyclized product **1** was obtained from 4-picolylamine and a Schiff base with 3-picolylamine. Likewise, the reaction of (2-aminophenyl)benzimidazole containing an amino group at a suitable (ortho) position to the benzimidazolyl −NH group with Fc-C was expected to form a cyclized quinazoline, while for aromatic 2,4,6-trimethylbenzene-1,3-diamine that contains amino groups at the 1 and 3 positions, only a Schiff base (**3**) was formed.

Crystal Structures. Crystal structures of **1**, **2**, and **4** have been authenticated by single-crystal X-ray diffraction analyses. **1** and **4** crystallize in a monoclinic crystal system with C_2/c and $P2_1/n$ space groups, while **2** is in an orthorhombic system with a *Pca*21 space group. The crystal structure of **1** revealed that it consists of two units each of ferrocene and 4-picolylamine, creating a five-membered imidazolidine ring with three chiral centers at the 2, 4, and 5 positions (Figure 1). The ferrocenyl units are located above and below the imidazolidine ring, while the pyridyl and picolyl rings oriented on the same side. The Cp ring of ferrocene (Fe1) is almost overlapping with the picolyl ring, with a centroid−centroid separation of ∼3.589 Å, and may be responsible for shielding the picolyl relative to the pyridyl

dx.doi.org/10.1021/ic201663m | *Inorg. Chem.* 2012, 51, 298−311

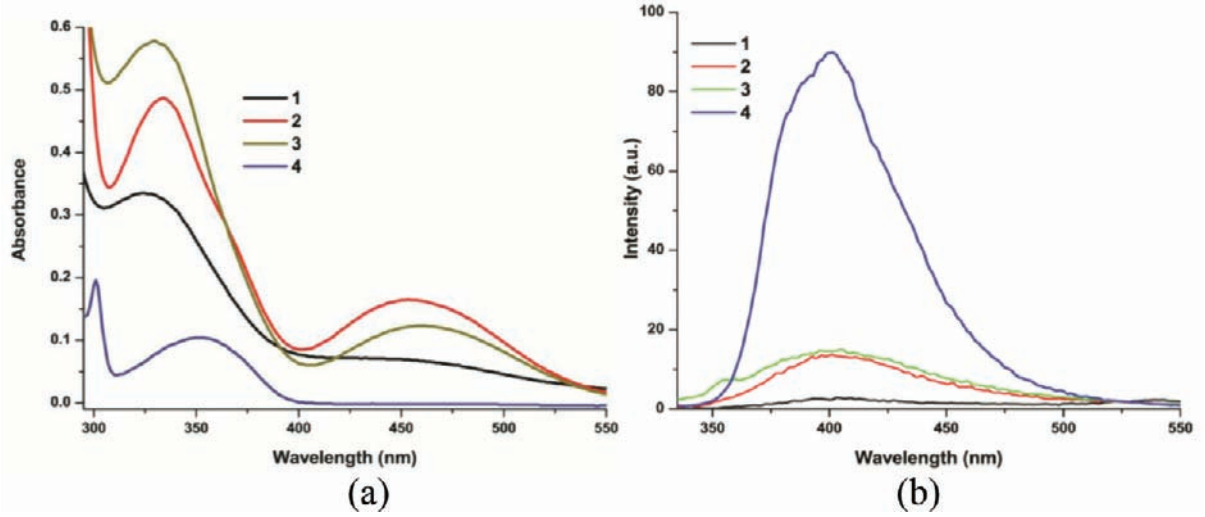

Figure 3. (a)Absorption and (b) emission (λ_{ex}, 320 nm for **2** and **3**; 325 nm for **1** and **4**; 500 V PMT) spectra of **1**–**4** in H_2O/EtOH (1:1, v/v; 10 μM).

ring protons (Figures 2a and S1 in the SI). The angles (C11–N2–C22, 103.70°; C18–C11–N2, 101.27°; N2–C22–N1, 101.99°; <120°) indicated the creation of a nonplanar five-membered ring. The pyridyl and picolyl substituents moved out of the adjacent ferrocenyl plane to avoid steric crowding (C9–C22–N2–C11, −165.34°; C13–C11–N2–C22, −79.87°; C16–C18–C11–C13, −143.42°; C22–N1–C18–C16, −122.91°). Further, it lacks hydrogen-bonding interactions; however, one of the substituted ferrocenyl groups (Fe2) is fixed by a set of intermolecular $\pi\cdots\pi$ interactions (C7···C14, 3.155 Å; Figure S6 in the SI, top). The C–H···π interactions along the crystallographic *c* and *a* axes resulted in helical and spherical motifs (Figures 2b and S6 in the SI, bottom), and the C–H···C distances (C23–H23···C15, 2.794 Å; C28–H28···C29, 2.863 Å) are in accordance with the reported values.[24]

The crystal structure of **2** represents a Schiff base containing one unit each of ferrocene and 3-picolylamine (Figure 1). The aldimine bond distance and angle [C11–N2, 1.266(3) Å; C11–N2–C13, 116.53°] suggested that –C═N– lies in the same plane as the substituted Cp ring of the ferrocene. It lacks intra/intermolecular hydrogen-bonding and $\pi\cdots\pi$ interactions, while C–H···π intermolecular interactions lead to linear chains with the hexagonal cavity along the crystallographic *a* axis (Figure S7 in the SI). In **4** (Figure 1c), the ferrocenyl unit is almost perpendicular to the phenylbenzimidazole ring plane (dihedral angles: C13–N3–C14–C15, 78.53°; C7–N2–C14–C15, −90.08°) to avoid steric crowding. The aminophenyl ring resides in the same plane as the benzimidazole ring, with a slight bending of the N3 nitrogen atom from the quinazoline ring. The C–N bond distances C14–N3 and C14–N2 are 1.456(6) and 1.464(6) Å, while the angle N3–C14–N2 is 105.5(4)°, suggesting sp^3 hybridization at C14. The bond angles N2–C14–C15 and N3–C14–C15 are 109.5(3) and 116.6(4)°, respectively. Compound **4** lacks both hydrogen-bonding and $\pi\cdots\pi$ interactions, while intermolecular C–H···π interactions are present between C4–H4···C16, C4–H4···C17, and C18–H18···C1 atoms (Figure S8 in the SI).[24]

■ ELECTRONIC SPECTROSCOPY

Electronic absorption spectra of **1**–**4** (H_2O/EtOH, 1:1, v/v) exhibited prominent bands at ~325–462 nm. The high-energy intense bands (325 nm, 0.333 × 10^5 M^{-1} cm^{-1}, **1**; 334 nm, 0.484 × 10^5 M^{-1} cm^{-1}, **2**; 330 nm, 0.572 × 10^5 M^{-1} cm^{-1}, **3**; 351 nm, 0.155 × 10^5 M^{-1} cm^{-1}, **4**; Figure 3a) have been assigned to ligand-centered π–π* transitions and the weak low-energy bands (451 nm, 0.067 × 10^5 M^{-1} cm^{-1}, **1**; 454 nm, 0.164 × 10^5 M^{-1} cm^{-1}, **2**; 462 nm, 0.123 × 10^5 M^{-1} cm^{-1}, **3**; 445 nm, 0.006 × 10^5 M^{-1} cm^{-1}, **4**) to either metal-to-ligand charge-transfer (MLCT; dπ–π*) or d–d transitions.[25] Notably, **4** exhibited a weak absorption band at 445 nm (Figure S9a in the SI) only at higher concentrations (1.0 mM).

Visual Detection of Hg^{2+} and Pb^{2+} Ions. The compounds under investigation (**1**–**4**) give a colored solution and are expected to show color changes upon interaction with various metal ions, which may form the basis for "naked eye" visible detection. In this context, solutions of **1**–**4** in H_2O/EtOH (1:1, v/v; 100 μM) were treated with various metal ions (*c*, 10 mM), viz., Na^+, K^+, Mg^{2+}, Ca^{2+}, Fe^{2+}, Co^{2+}, Ni^{2+}, Cu^{2+}, Zn^{2+}, Cd^{2+}, Pb^{2+}, Ag^+, and Hg^{2+} (10.0 equiv). Compounds **1**–**3** do not show any significant color changes in the presence of added metal ions. However, the addition of Hg^{2+}/Pb^{2+} (2.0 equiv) to a solution of **4** leads to "naked-eye" visible color changes that turned to dark red/light green (from light yellow) at higher concentrations (10.0 equiv) of these ions (Figures 4 and S9b in the SI). Further, the addition of an excess of Cu^{2+} (10.0 equiv) to a solution of **4** also leads to light-brown color; however, its electronic spectra do not show any noticeable shift in the position of absorption bands (Figures 4 and 5a). The colorimetric response toward the Hg^{2+} and Pb^{2+} ions persisted under an aqueous environment for longer periods (>72 h), suggesting that **4** can act as a potential chromogenic sensor for Hg^{2+} and Pb^{2+} ions.

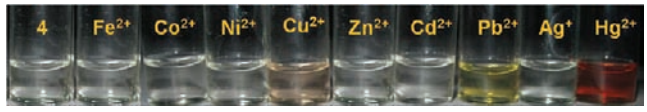

Figure 4. Changes in the color of 100 μM solutions of **4** with 10.0 equiv (10 mM) of some selected interferring metal ions in a H_2O/EtOH (1:1, v/v) solution.

Metal-Ion-Sensing Behavior. The metal-ion-complexing performance of **1**–**4** has been followed in H_2O/EtOH (1:1, v/v; 10 μM) by absorption and emission spectral studies. Electronic absorption spectra of **1**–**3** (10 μM; Figure S10 in the SI) do not show any substantial change in the presence of 10.0 equiv of various metal ions (*c*, 10 mM), viz., Li^+, Na^+, Ca^{2+}, Mg^{2+}, Fe^{2+},

dx.doi.org/10.1021/ic201663m | *Inorg. Chem.* 2012, 51, 298–311

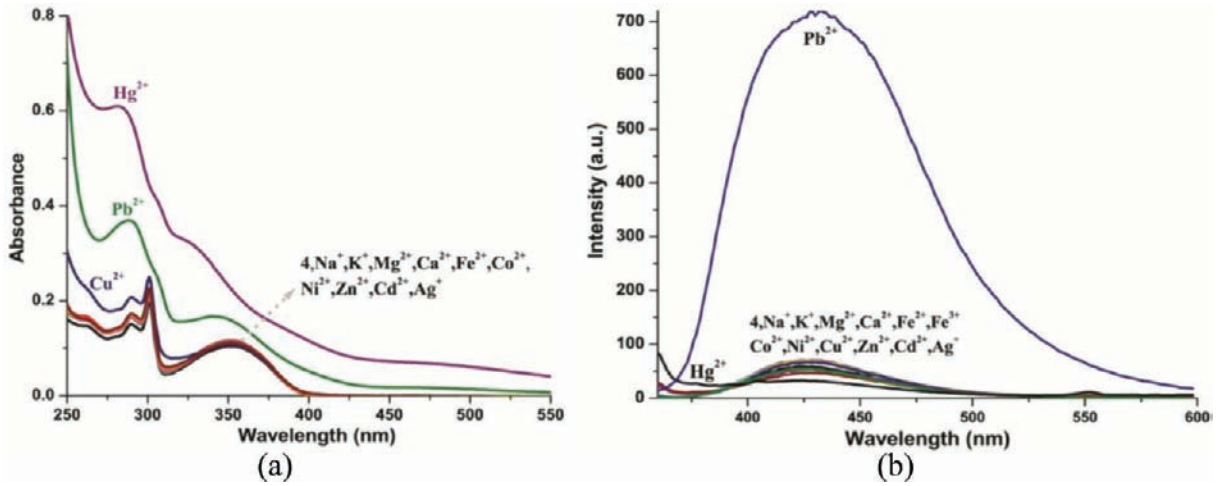

Figure 5. Absorption (a) and fluorescence (b) spectra of probe **4** (*c*, 10 μM) in the presence of various metal ions (10.0 equiv; *c*, 10 mM) in H_2O/EtOH (1:1, v/v).

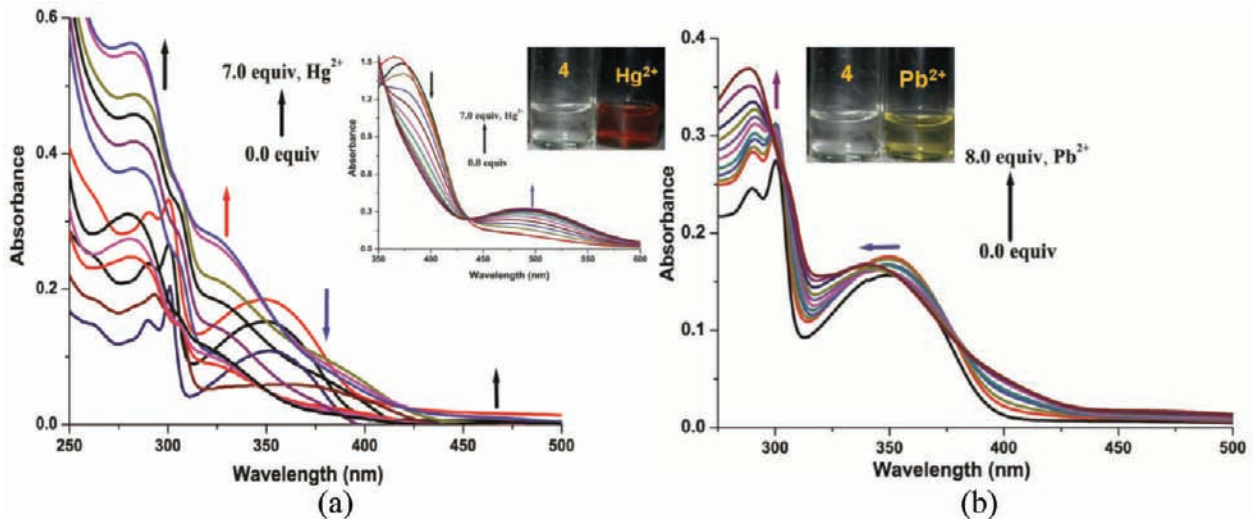

Figure 6. (a) Absorption titration spectra of probe **4** (*c*, 10 μM) in the presence of various equivalents of $Hg(NO_3)_2$ (0.0−7.0 equiv; *c*, 10 mM). Insets: (i) absorption titrations of **4** (*c*, 500 μM) with Hg^{2+} (0.0−7.0 equiv; *c*, 100 mM); (ii) naked eye color distinction between **4** and **4** in the presence of Hg^{2+}. (b) Absorption titration spectra of **4** (*c*, 10 μM) with Pb^{2+} (0.0−8.0 equiv; *c*, 10 mM) in 1:1 (v/v) H_2O/EtOH. Inset: naked eye color change between **4** and **4** in the presence of Pb^{2+}.

Co^{2+}, Ni^{2+}, Cu^{2+}, Zn^{2+}, Cd^{2+}, Pb^{2+}, and Hg^{2+}. However, the addition of Hg^{2+} and Pb^{2+} ions to a solution of **1** and **2** led to hyperchromic shifts (Figure S10a,b in the SI; 0.333×10^5 to 0.561×10^5 M^{-1} cm^{-1}, **1**; 0.484×10^5 to 0.552×10^5 M^{-1} cm^{-1}, **2**), while **3** (330 nm; ε, 0.572×10^5 M^{-1} cm^{-1}) exhibited a small red shift (340 nm; 0.625×10^5 M^{-1} cm^{-1}) in the presence of Ag^+ ions (Figure S10c in the SI). On the other hand, among the tested metal ions, the addition of an excess of Hg^{2+} (10.0 equiv) to a solution of **4** results in an appreciable blue shift ($\Delta\lambda$ = 26 nm) in the position of the low-energy band (325 nm, 0.323×10^5 M^{-1} cm^{-1}; Figure 5a) along with the appearance of a new weak band at 480 nm (ε, 0.065×10^5 M^{-1} cm^{-1}). Further, the high-energy (301 nm; 0.222×10^5 M^{-1} cm^{-1}) and low-energy bands (351 nm; 0.155×10^5 M^{-1} cm^{-1}) of **4** illustrated blue shifts upon the addition of Pb^{2+} ions (288 nm, 0.373×10^5 M^{-1} cm^{-1}; 342 nm, 0.168×10^5 M^{-1} cm^{-1}). Other tested metal ions do not show any appreciable change in the position of the absorption bands.

To understand the binding affinity of the tested metal ions, titration experiments have been performed. The addition of Hg^{2+} (0.5 equiv) to a solution of **4** (H_2O/EtOH, 1:1, v/v; 10 μM) causes a concomitant decrease and increase in the optical density of low- and high-energy bands at 351 and 301 nm, respectively (Figure 6a), and the color of the solution turns light red. An increase in the concentration of the Hg^{2+} ion (1.0 equiv) leads to a decrease in the optical density along with gradual red and blue shifts of the low-energy (359 nm, 0.081×10^5 M^{-1} cm^{-1}) and high-energy (282, $\Delta\lambda$, 19 nm) bands, respectively. Further additions of Hg^{2+} (5.0−6.0 equiv) cause the disappearance of the band at 359 nm and the emergence of new bands at 480 ($\Delta\lambda$, 35 nm), 321 ($\Delta\lambda$, 30 nm), and 282 nm ($\Delta\lambda$, 19 nm), and the color of the solution turns dark red. It is also observed that, in titration experiments involving higher concentrations of **4** (*c*, 500 μM), the band centered at 480 nm intensifies (ε, 0.331×10^5 M^{-1} cm^{-1}). Moreover, the appearance of an isosbestic point at 435 nm suggested the presence of more than two species in the reaction medium (Figure 6a). Significant changes in the absorption spectra may be attributed to the formation of a mercury complex.[26] Job's plot analysis at 480 nm revealed 1:1 stoichiometry for **4** and Hg^{2+} (Figure S11a in the SI). Likewise, Pb^{2+} ion interaction studies were carried out in the same solvent system (Figure 6b). The

dx.doi.org/10.1021/ic201663m | *Inorg. Chem.* 2012, 51, 298−311

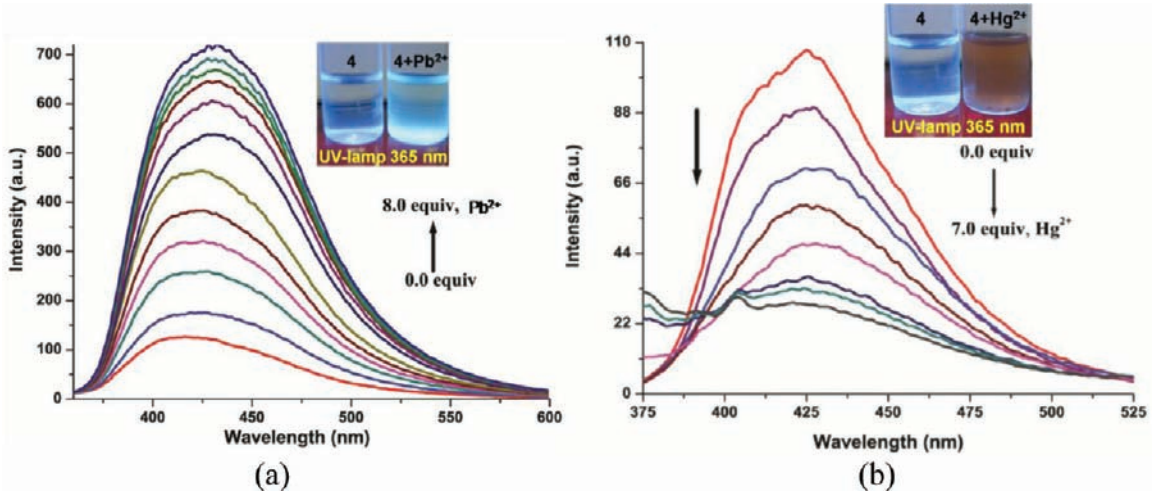

Figure 7. Fluorescence titration spectra of probe **4** (c, 10 μM) in the presence of (a) Pb^{2+} (0.0−8.0 equiv; c, 10 mM) and (b) Hg^{2+} (0.0−7.0 equiv; c, 10 mM) in H_2O/EtOH (1:1, v/v). Insets: comparative fluorescence intensity of **4**/**4** + Pb^{2+} and **4**/**4** + Hg^{2+} under a UV lamp irradiated at 365 nm.

absorbance of the bands associated with both low (351 nm, 0.176×10^5 M^{-1} cm^{-1}) and high (301 nm, 0.312×10^5 M^{-1} cm^{-1}) energy significantly increases upon the addition of 0.5 equiv of Pb^{2+} ion. Further additions of Pb^{2+} (1.0−8.0 equiv) lead to a blue shift of both low-energy ($\Delta\lambda$, 9 nm) and high-energy ($\Delta\lambda$, 13 nm) bands to appear at 342 and 288 nm, and the color of the solution turns light green. The isosbestic points at 333 and 381 nm suggested the presence of more than two species and sensitivity of the system for the metal ion.[26] Job's plot analysis at 351 nm revealed 2:1 stoichiometry for **4** and Pb^{2+} (Figure S11b in the SI). Competitive metal-ion selectivity experiments have been carried out by the addition of the tested metal ions (10.0 equiv) to a solution containing **4** + Hg^{2+} and observed that the band due to **4** + Hg^{2+} remains unaffected except for Pb^{2+} (Figure S12a in the SI). The positions of the low-energy bands exhibited insignificant red (∼1 nm) and hypochromic (ε, 0.263×10^5 M^{-1} cm^{-1}) shifts upon the addition of Pb^{2+} ions. Similarly, the addition of various metal ions (10.0 equiv) to a solution containing **4** + Pb^{2+} displayed no change except for Hg^{2+}, which induces a blue shift ($\Delta\lambda$, ∼18 nm) of the low-energy band (326 nm; ε, 0.212×10^5 M^{-1} cm^{-1}; Figure S12b in the SI). The new band corresponds to **4** + Hg^{2+}, suggesting displacement of the Pb^{2+} ion from the **4** + Pb^{2+} complex. The association constants for Hg^{2+} and Pb^{2+} could not be estimated from absorption data because of a persistent shift in the absorption titration curve. The overall result suggested stronger interaction of **4** toward Hg^{2+} relative to Pb^{2+} ions under analogous conditions.

Among the compounds under study (H_2O/EtOH; 1:1, v/v; c, 10 μM), **1**−**3** (λ_{ex} is 325 nm for **1** and 320 nm for **2** and **3**) exhibit weak fluorescence at ∼401−405 nm (500 V PMT; Figure 3b); however, **4** displays relatively high fluorescence at 427 nm (Φ, 0.26; pyrene; λ_{ex}, 325 nm).[27] The cyclic compound **1** fluoresces weakly because of rupture of the electronic conjugation at chiral centers 2, 4, and 5, while Schiff bases **2** and **3** are due to the lack of planarity and the photoinduced electron-transfer process. The high fluorescence behavior of **4** may be attributed to its extended conjugation in the planar phenylbenzimidazole chromophore because benzoannulated benzimidazole derivatives usually exhibit intense fluorescence and optoelectronic properties.[28] The fluorescence behavior of **1**−**4** has also been examined in the presence of tested metal ions, and it is observed that **1**−**3** did not show any substantial change (Figure S13 in the SI). In contrast, **4** displayed notable fluorescence enhancement and quenching in the presence of Pb^{2+} and Hg^{2+} ions, respectively (Figure 5b). To understand the binding affinity of **4** toward Hg^{2+}, fluorescence titration experiments were performed (Figure 7b). The addition of Hg^{2+} (0.5 equiv) to a solution of **4** (10 μM) induced a decrease (17%) in its emission intensity. The limit of quantification for Hg^{2+} in the solution of **4** was ∼1.0:0.5 to 1.0:7.0, and maximum fluorescence quenching (72%) was observed at a ∼1.0:7.0 (**4**/Hg^{2+}) ratio with a reduced quantum yield (Φ, 0.08; $\Delta\Phi$, 0.18). Detectable fluorescence quenching of **4** in the presence of Hg^{2+} under a UV lamp (365 nm) is depicted in Figure 7 (inset). The observed quenching may be attributed to the interaction of **4** with Hg^{2+} and/or the chelation-enhanced quenching effect.[9b,29a−e] Job's plot analysis showed 1:1 (**4**/Hg^{2+}) stoichiometry (Figure S14a in the SI), and the quenching constant derived from the Stern−Volmer plot was K_{sv} = 51 840 M^{-1} (Figure S15 in the SI). To ascertain the applicability of **4** as a selective fluorescent chemosensor for the Hg^{2+} metal ion, competition studies were performed and monitored by fluorescence spectral studies. The addition of tested metal ions (10.0 equiv) to a solution of **4** + Hg^{2+} exhibited a modest enhancement (16%) in the presence of Pb^{2+} only, while other cations were ineffective in this regard (Figure S16a in the SI).

To gain further insight into the complexation and potential photophysical, *turn-on* switching behavior of **4** with a Pb^{2+} fluorescence titration experiment was performed. A change in the fluorescence intensity of **4** in the presence of Pb^{2+} and a detectable response under a UV lamp (365 nm) are depicted in Figure 7a. The fluorescence intensity was significantly enhanced upon the addition of Pb^{2+} (0.5 equiv, 13%). The quantum yield increased by a factor of 2.5 (Φ = 0.69), and the intensity assumed its maximum (∼7-fold) by adding ∼8.0 equiv of Pb^{2+}. This observation is consistent with the conclusions drawn from UV−vis spectral studies and may be attributed to chelation-enhanced fluorescence (CHEF).[29f−h,30] Job's plot analysis suggested 2:1 (**4**/Pb^{2+}) stoichiometry (Figure S14b in the SI). Association constants for **4** + Hg^{2+} and **4** + Pb^{2+} have been calculated by the Benesi−Hildebrand method and found to be 1.39×10^4 and 2.52×10^2 mol^{-1}, respectively (Figure S17 in the SI).[31] The selectivity of **4** toward Pb^{2+} was also examined by interference studies, and it was observed that none of the tested metal ions (10.0 equiv) leads to significant changes except Hg^{2+}, which induces considerable fluorescence quenching (37%; Figure S16b in the SI). The overall results suggest that **4** selectively detects the Hg^{2+} and Pb^{2+} ions with distinct output signaling and shows higher selectivity for Hg^{2+} over Pb^{2+} in aqueous media (Figures S12

dx.doi.org/10.1021/ic201663m | *Inorg. Chem.* 2012, 51, 298−311

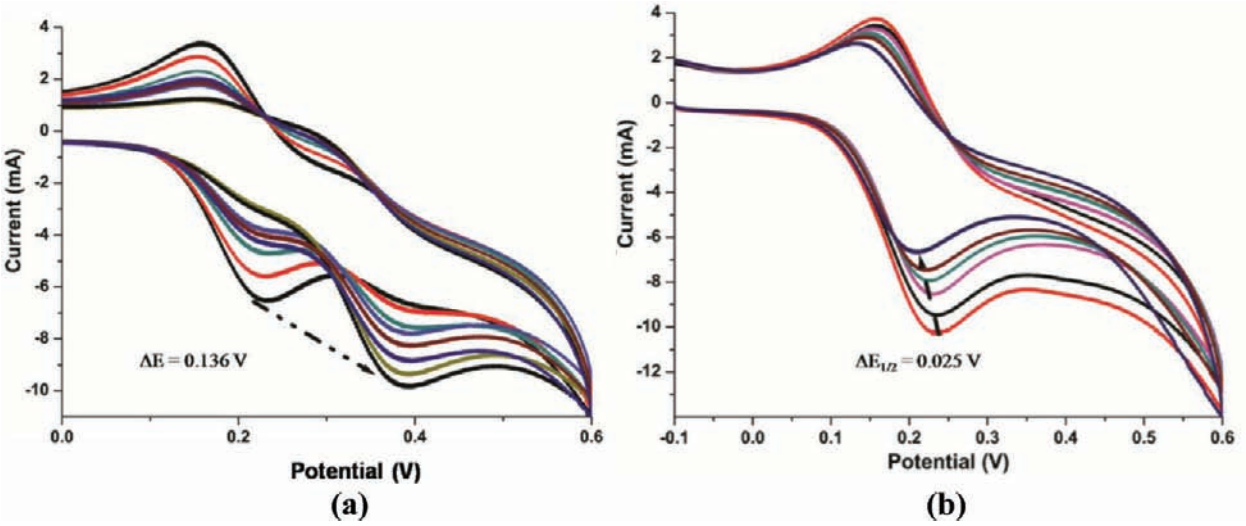

Figure 8. Cyclic voltammetric titrations of **4** (H_2O/EtOH, 1:1, v/v; *c*, 100 μM) in the presence of (a) Hg^{2+} (100 mM) and (b) Pb^{2+} (100 mM) at room temperature.

and S16 in the SI). The selectivity of **4** for Pb^{2+} over Ca^{2+}, Zn^{2+}, Cd^{2+}, and Fe^{2+} is particularly important because Pb^{2+} targets both Ca^{2+} and Zn^{2+} binding sites in vivo and Cd^{2+}, Hg^{2+}, and Fe^{2+} metal ions that frequently interfere with Pb^{2+} analysis.[32] Finally to check the effect of acid/base on the optical behavior of **4**, an excess each (5.0 equiv) of 1.0 M HNO_3 and 1.0 M KOH was added to its solution, which led to insignificant changes in the fluorescence behavior of **4** (Figure S18 in the SI).

Electrochemical Studies. The ferrocene unit attached to a particular system can serve as a molecular scaffold, sensitive probe, chromophore, redox-active and catalytic site, etc.[11m] The reversibility and redox behavior of **1**−**4** in the presence of various metal ions have been investigated by cyclic voltammetry in H_2O/EtOH (1:1, v/v; *c*, 100 μM) at room temperature using 0.1 M $[(n\text{-Bu})_4N]ClO_4$ as a supporting electrolyte. In the anodic potential window (0−2.0 V), **1**−**4** displayed distinct oxidative responses (Figure S19 in the SI). The cyclic voltammogram of **1** exhibited somewhat overlapped reversible double-wave oxidations (Figure S19a in the SI) at E_{pa} = 0.50 and 0.75 V [ΔE ($E_{pa} - E_{pc}$) = 0.09 and 0.17 V] at a scan rate of 0.1 V s^{-1}. On the other hand, **2**−**4** displayed reversible single oxidation waves at E_{pa} = 0.38 (ΔE = 0.13), 0.34 (ΔE = 0.10), and 0.26 V (ΔE = 0.08 V), respectively. The oxidative responses in these compounds are within the range for ferrocene derivatives, and oxidation process is more facile in **2**−**4** in comparison to **1**.[33,34] It is noteworthy that both **1** and **3** contain two ferrocenyl units and the former displays two and the latter only one reversible oxidation wave assignable to the Fc/Fc^+ redox couple. It may be attributed to the symmetrical structure of **3**, wherein the electronic environments about both of the Fe^{II} centers are equivalent. On the other hand, in unsymmetrical compound **1**, the electronic environment about the Fe^{II} centers is nonequivalent because these are substituents of the newly created five-membered imidazolidine ring (Figure 1). The single wave observed for **1**−**4** (Figure S20 in the SI) in the cathodic potential window may be attributed to ligand-based reductions.

The metal-ion interaction studies on **1**−**4** in H_2O/EtOH (1:1, v/v; *c*, 100 μM) have been investigated by cyclic voltammetry in the presence of various metal ions (Na^+, K^+, Mg^{2+}, Ca^{2+}, Fe^{2+}, Co^{2+}, Ni^{2+}, Cu^{2+}, Zn^{2+}, Cd^{2+}, Pb^{2+}, Ag^+, and Hg^{2+}). **1**−**3** (100 μM) do not show any significant changes in the presence of tested metal ions (100 mM; Figure S21 in the SI); however, **4** (100 μM) exhibited substantial changes in the presence of Hg^{2+} and Pb^{2+} ions, respectively (Figure S21 in the SI). Independently and in the presence of metal ions, **2**−**4** displayed single waves (oxidative), while **1** displayed somewhat overlapping double waves corresponding to different electronic environments about the ferrocenyl units. To gain a deeper insight into the sensitivity and mechanism of selective detection of Hg^{2+} and Pb^{2+} ions, electrochemical titrations have been performed (Figure 8). The addition of Hg^{2+} (0.5 equiv) to a solution of **4** led to a decrease in the current intensity of the oxidation wave (ΔI = 16%). A further increase in the concentration of Hg^{2+} (1.0−5.0 equiv) leads to a decrease in the current intensity of the oxidation wave due to **4** at E_{pa} = 0.26 V with the appearance of a new irreversible single wave at +0.395 V (ΔE_{pa} = 0.136 V; Figure 8a). The reversible wave associated with **4** finally vanishes, and an irreversible single wave appears at a more positive potential, suggesting selective electrochemical sensing of **4** toward the Hg^{2+} ion. The observed positive potential shift of the Fc/Fc^+ redox wave in the presence of Hg^{2+} may be attributed to the electrostatic repulsion between the bound metal ion and the electrogenerated positive charge on the oxidized ferrocene unit. This reduces the association constant with the oxidized ligand and leads to destabilization of the complex.[25,33] Thus, ΔE_{pa} reflects the balance of metal-ion interaction between neutral and oxidized ligands.[35] Likewise, the addition of Pb^{2+} (0.5−5.0 equiv) to a solution of **4** induced a noticeable decrease in the current intensity along with a small negative potential shift (ΔE_{pa} = 0.025 V; Figure 8b). The observed shift indicates that the Pb^{2+} ion promoted oxidation of the free probe. Further, to ascertain that electrochemical changes in the presence of Hg^{2+}/Pb^{2+} are not due to variation in the pH, 1.0 M of aqueous HNO_3 and KOH were added to a solution of **4** (5.0 equiv; Figure S18c in the SI). It was observed that the addition of acid/base does not cause any significant change of the position of the single wave. The overall electrochemical results suggested that both Hg^{2+} and Pb^{2+} interact with **4**; however, Hg^{2+} binds more strongly than Pb^{2+}. The changes in the cyclic volammograms in the presence of Hg^{2+}/Pb^{2+} corroborated well with the conclusions drawn from UV−vis titration studies.

MS Studies. The formation of **1**−**4** and the binding behaivor of **4** with Hg^{2+}/Pb^{2+} ions have further been supported by mass spectrometry (DART-MS and HRMS) studies. The DART-MS of **1**−**4** displayed molecular ion peaks at *m*/*z* 609.2433 (M^+ + 1; **1**),

dx.doi.org/10.1021/ic201663m | *Inorg. Chem.* 2012, 51, 298−311

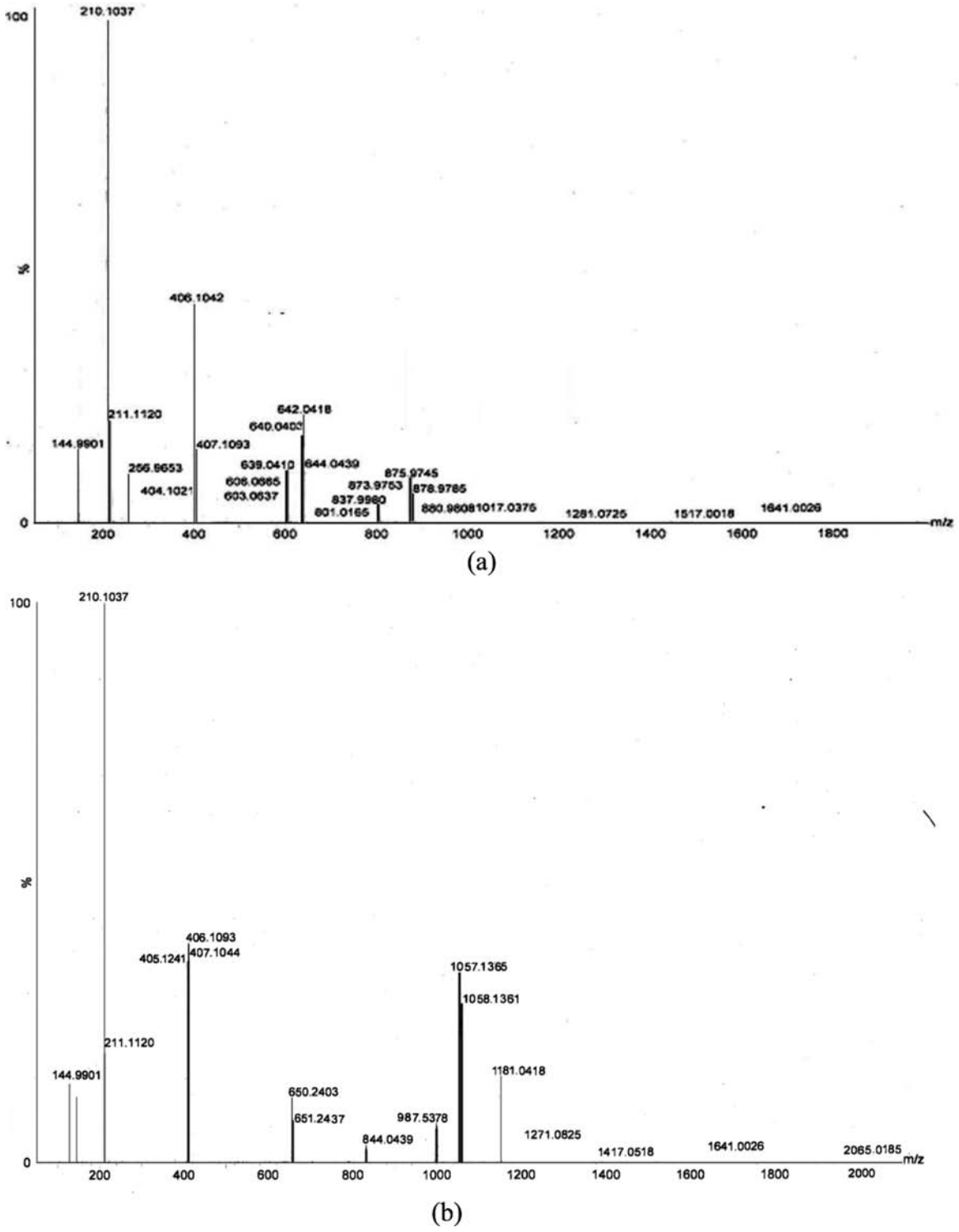

Figure 9. HRMS spectra of (a) **4** + Hg^{2+} and (b) **4** + Pb^{2+} in DMSO.

305.1139 (M^+ + 1; **2**), 543.2184 (M^+ + 1; **3**), and 406.1164 (M^+; **4**), which strongly supported formulation of the respective compounds (Figure S22 in the SI). Prominent peaks at *m*/*z* 837.9980 and 642.0418 (calcd 837.1002 and 642.1243) corresponding to $[\mathbf{4}\cdot\{Hg(NO_3)_2\}(H_2O)_2\cdot 4H_2O]^+$ and $[\mathbf{4}\cdot\{Hg(H_2O)_2\}^{2+}]^+$ (Figure 9a) were displayed in the MS spectrum of **4** + Hg^{2+}. The presence of a strong peak at *m*/*z* 642 suggested coordination of at least two H_2O molecules with the metal center. It is worth mentioning that we could not observe a peak due to $[\mathbf{4}\cdot\{Hg(NO_3)(H_2O)_2\}^+]^+$, probably because of weaker interaction between the mercury and nitrate ions through oxygen. This has been supported by theoretical studies. Similarly, the MS spectrum of **4** + Pb^{2+} exhibited a peak at *m*/*z* 1057.1365 (calcd 1056.2423) corresponding to isotopic $(M + 1)^+$ 2:1 complex $[\mathbf{4}_2\cdot Pb(H_2O)_2]^+$ (Figure 9b). The overall high-resolution mass spectral (HRMS) studies supported the binding of **4** with Hg^{2+} and Pb^{2+} ions.

^{1}H NMR Titration Studies. ^{1}H NMR titration studies (DMSO-d_6) have been made to explore possible binding sites of **4** with Hg^{2+}/Pb^{2+} ions. The NMR spectral changes in **4** were not clearly detectable upon the addition of 0.1 equiv of Hg^{2+}/Pb^{2+}

dx.doi.org/10.1021/ic201663m | *Inorg. Chem.* 2012, 51, 298−311

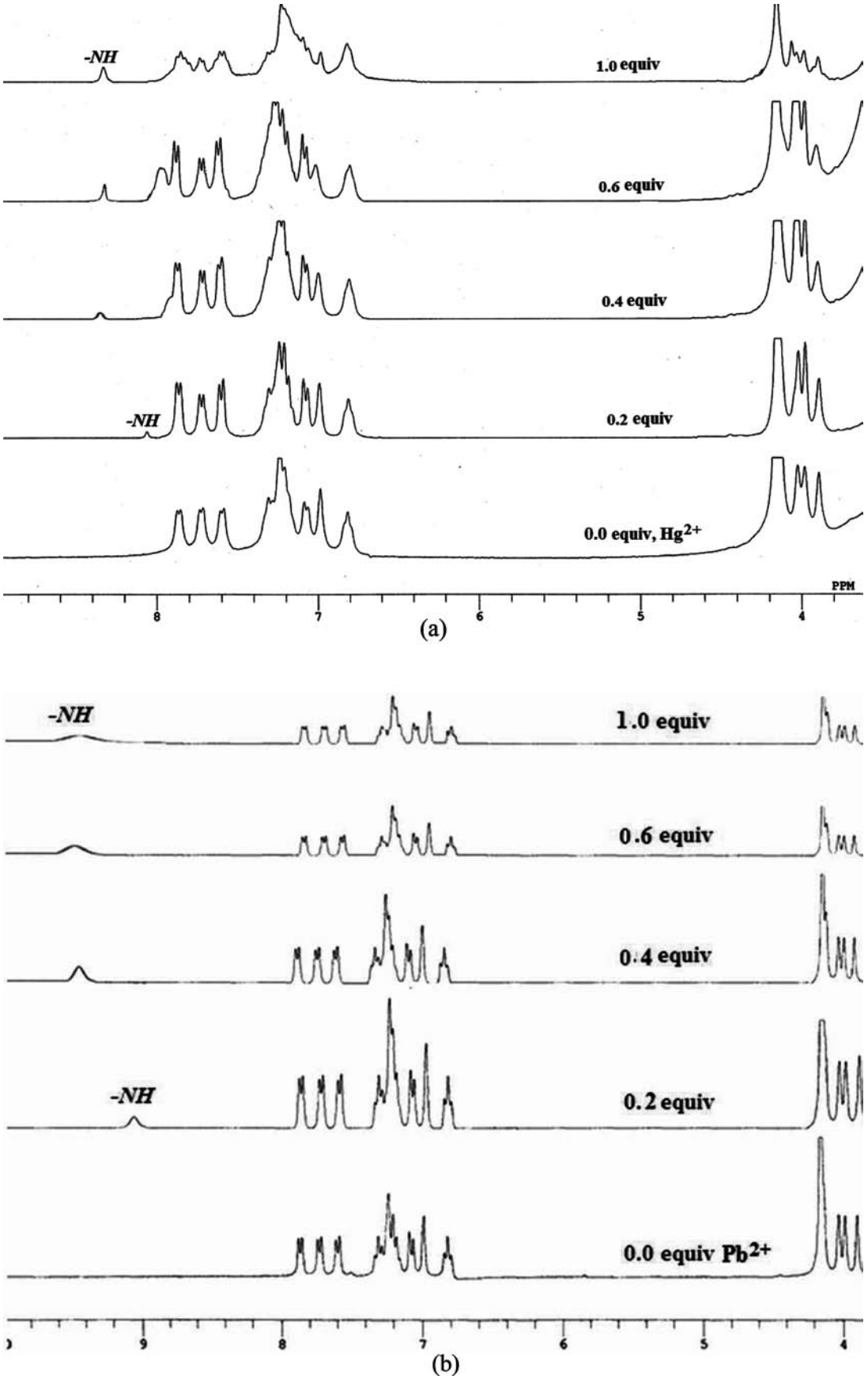

Figure 10. Partial ^{1}H NMR titration spectra (stacked) of **4** in the presence of Hg^{2+} (a) and Pb^{2+} (b) at room temperature in DMSO-d_6.

ions. However, the addition of 0.2 equiv of Hg^{2+} induces a noticeable downfield shift ($\Delta\delta$, 0.80 ppm) of the quinazoline ring proton (δ 7.29) H9 to appear at δ 8.09 (Figure 10a). An increase in the concentration of Hg^{2+} (0.4 equiv) leads to a

dx.doi.org/10.1021/ic201663m | *Inorg. Chem.* 2012, 51, 298–311

further downfield shift of the H9 proton (δ 8.32; $\Delta\delta$, 1.03 ppm). Further, the singlet corresponding to H9 becomes intense and broad without a substantial shift ($\Delta\delta$, 1.05 ppm) upon the addition of 0.6−1.0 equiv of Hg^{2+}. It indicated interaction of Hg^{2+} through the −NH nitrogen-donor site of the probe **4** (Figure 11). Similarly, the signal due to H9 exhibited a significant

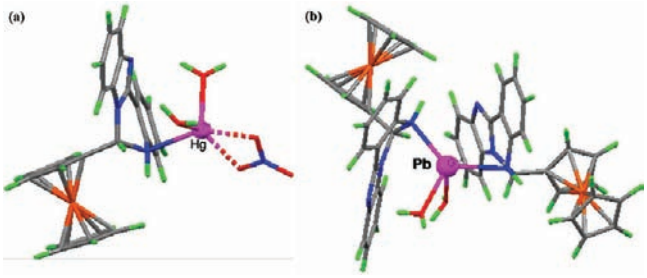

Figure 11. Calculated (6-31G**/LANL2DZ) structure for **4** + Hg^{2+} (a) and **4** + Pb^{2+} (b) complexes, in capped sticks for clarity.

downfield shift upon the addition of Pb^{2+} (0.2 equiv) and appeared at δ 9.06 ($\Delta\delta$, 1.77 ppm; Figure 10b). Upon an increase in the concentration of Pb^{2+} (0.4 equiv), the downfield shift due to the H9 proton becomes more pronounced (δ 9.47; $\Delta\delta$, 2.18 ppm). This suggested interaction of **4** with Pb^{2+} only through the −NH nitrogen-donor site. These observations are consistent with the conclusions drawn from absorption and emission spectral studies.

The plausible mechanisms for chromogenic, fluorogenic, and electrochemical changes in **4** in the presence of Hg^{2+}/Pb^{2+} ions have been proposed on the basis of UV−vis, fluorescence, electrochemical, HRMS, and ^{1}H NMR titration studies and Job's plot analysis. The observed red shift of the absorption bands due to **4** in the presence of Hg^{2+} may be attributed to the formation of Mercury (II) complex in 1:1 stoichiometry (Figures 11a and S11 and S14 in the SI). The fluorescence quenching may be ascribed to changes in the geometry of the probe upon interaction with Hg^{2+} through the −NH nitrogen-donor site of the probe, which has been supported by ^{1}H NMR titration studies (Figures 10a and 11a).[9b,29a−e] Unlike **4** + Hg^{2+}, the absorption band of **4** exhibited a relatively small shift in the presence of Pb^{2+}. It is reasonable to think that interaction of **4** with Pb^{2+} through the −NH nitrogen atom of the quinazoline ring (Figures 10b and 11b) will not significantly affect delocalization in phenylbenzimidazole. This has been supported by ^{1}H NMR titration studies, where none of the aromatic protons exhibited a significant shift. The fluorescence enhancement observed for **4** in the presence of Pb^{2+} may be ascribed to CHEF,[29f−h] wherein the probe retains its planarity and donor atoms adopt a tetrahedral arrangement about the metal center in 2:1 (**4**/Pb^{2+}) stoichiometry (Figures 9, 11b, and S14 in the SI).[33] The significant positive potential shift with Hg^{2+} (0.136 V) and the small negative shift in the presence of Pb^{2+} (0.025 V) in the cyclic volammogram also indicated different interaction modes of **4** with Hg^{2+} and Pb^{2+} ions.

Quantum-Chemical Calculations. Further, to support our viewpoint toward the mode of interaction, quantum-chemical calculations have been performed on complexes of **4** with Hg^{2+}/Pb^{2+} ions. This indicated that the only coordinating site is the −NH nitrogen-donor atom of the quinazoline ring. In the 1:1 (**4** + Hg^{2+}) complex, the −NH nitrogen-donor atom of the quinazoline ring, two H_2O molecules, and a nitrate ($-NO_3$) are tetrahedrally arranged around the Hg^{2+} ion (Figure 11a). On the other hand, in the 2:1 (**4** + Pb^{2+}) complex, two −NH nitrogen-donor atoms of the quinazoline ring from two distinct molecules of **4** and two H_2O molecules are coordinated in a tetrahedral fashion (Figure 11b). These binding patterns are in accordance with the experimental predictions based on the spectral studies.

CONCLUSIONS

Through this work, we have presented one-pot synthesis and characterization of four new ferrocene derivatives **1**−**4**. It has been established that **1**−**3** are nonfluorescent, while **4** displays moderate fluorescence and chromogenic, fluorogenic, and electrochemical sensing selectively toward Hg^{2+} and Pb^{2+} ions. Job's plot analysis supported 1:1 and 1:2 stoichiometries between **4** and Hg^{2+}/Pb^{2+} ions, respectively. The mode of interaction between Hg^{2+}/ Pb^{2+} and **4** has been supported by ^{1}H NMR spectroscopic and MS studies and verified by theoretical studies. It presents the first report dealing with application of a ferrocene/quiazolidine as a chemosensor for Hg^{2+}/Pb^{2+} through chromogenic, fluorogenic, and electrochemical responses.

ASSOCIATED CONTENT

Supporting Information

X-ray crystallographic data of **1**, **2**, and **4** in CIF format, ^{1}H and ^{13}C NMR and 2D (^{1}H−^{13}C) spectra, $\pi\cdots\pi$ and C−H$\cdots\pi$ interactions, absorption and fluorescence graphs, B−H plots for the binding constant, DART-MS, and cyclic voltammograms. This material is available free of charge via the Internet at http://pubs.acs.org.

AUTHOR INFORMATION

Corresponding Author

*E-mail: dspbhu@bhu.ac.in. Phone: + 91 542 6702480. Fax: + 91 542 2368174.

ACKNOWLEDGMENTS

Thanks are due to the Department of Science and Technology (DST), New Delhi, India, for providing financial assistance through Scheme SR/S1/IC-15/2006. R.P. and M.S. are grateful to the Council of Scientific and Industrial Research (CSIR), New Delhi, India, for providing financial assistance in the form of a Senior Research Fellowship [9/13(288)/2010-EMR-I].

REFERENCES

(1) (a) *Fluorescent Chemosensors for Ion and Molecule Recognition*; Czarnik, A. W., Ed.; American Chemical Society: Washington, DC, 1993; p 1. (b) de Silva, A. P.; Gunaratne, H. Q. N.; Gunnlaugsson, T.; Huxley, A. J. M.; McCoy, C. P.; Rademacher, J. T.; Rice, T. E. *Chem. Rev.* **1997**, *97*, 1515−1566.

(2) (a) Metallol, C. M.; Heiden, M. G. V. *Genes Dev.* **2010**, *24*, 2717−2722. (b) Bartter, F. C.; Steinfeld, J. L.; Waldmann, T.; Delea, C. S. *Trans. Assoc. Am. Physicians* **1961**, *74*, 180−194. (c) Kim, B.-E.; Wang, F.; Dufner-Beattie, J.; Andrews, G. K.; Eide, D. J.; Petris, M. J. *J. Biol. Chem.* **2003**, *279*, 4523−4530. (d) Bressona, C.; Lamourouxa, C.; Sandrea, C.; Tabarantb, M.; Gaultc, N.; Poncyc, J. L.; Lefaixc, J. L.; Auwerd, C. D.; Speziae, R.; Gaigeote, M.-P.; Ansoborlof, E.; Mounicoug, S.; Frayssehe, A.; Devesh, G.; Bacquarth, T.; Sezneci, H.; Pouthieri, T.; Morettoi, P.; Ortegah, R.; Lobinskig, R.; Moulina, C. *Biochimie* **2006**, *88*, 1619−1629. (e) Zhao, Y.; Lin, K.; Zhang, W.; Liu, L. *J. Environ. Sci.* **2010**, *22*, 1987−1992. (f) Somerville, G. A.; Proctor, R. A. *Microbiol. Mol. Biol. Rev.* **2009**, *73*, 233−248. (g) Kim, S. R.;

Talbott, E. O.; Tull, E. S.; Zborowski, J. V.; Vogt, M. T.; Kuller, L. H. *Med. Hypotheses* **2002**, *59*, 655−659.
(3) (a) Šmirjáková, S.; Ondráovicová, O.; Kaŝková, A.; Laktiiová, K. *Folia Veterinaria* **2005**, *49*, S31−S32. (b) Bernard, A. *Indian J. Med. Res.* **2008**, *128*, 557−564. (c) Raikwar, M. K.; Kumar, P.; Singh, M.; Singh, A. *Veterinary World* **2008**, *1*, 28−30. (d) Xie, Y.; Trouba, K. J.; Liu, J.; Waalkes, M. P.; Germolec, D. R. *Environ. Health Perspect.* **2004**, *112*, 1255−1263. (e) Katz, S. A.; Katz, R. B. *J. Appl. Toxicol.* **1992**, *12*, 79−84. (f) Neal, R.; Aykin-Burns, N.; Ercal, N.; Zigler, J. S. Jr. *Taxicol.* **2005**, *212*, 1−9. (g) Kopf-Maier, P.; Kopf, H.; Neuse, E. W. *J. Cancer Res. Clin.* **1984**, *108*, 336−340. (h) Popova, L. V.; Babin, V. N.; Belousov, Y. A.; Nekrasov, Y. S.; Snegireva, A. E.; Borodina, N. P.; Shaposhnikova, G. M.; Bychenko, O. B.; Raevskii, P. M. *Appl. Organomet. Chem.* **1993**, *7*, 85−94.
(4) (a) Miller, J. R.; Rowland, J.; Lechler, P. J.; Desilets, M.; Hsu, L. C. *Water, Air, Soil Pollut.* **1996**, *86*, 373. (b) Huang, J.; Xu, Y.; Qian, X. *J. Org. Chem.* **2009**, *74*, 2167−2170. (c) Guliyev, R.; Coskun, A.; Akkaya, E. U. *J. Am. Chem. Soc.* **2009**, *131*, 9007−9013. (d) Wu, D. Y.; Huang, W.; Lin, Z. H.; Duan, C. Y.; He, C.; Wu, S.; Wang, D. H. *Inorg. Chem.* **2008**, *47*, 7190−7201. (e) Pacyna, E. G.; Pacyna, J. M.; Steenhuisen, F.; Wilson, S. *Atmos. Environ.* **2006**, *40*, 4048−4063. (f) Tchounwou, P. B.; Ayensu, W. K.; Ninashvili, N.; Sutton, D. *Environ. Toxicol.* **2003**, *18*, 149.
(5) Clarkson, T. W.; Magos, L.; Myers, G. J. *N. Engl. J. Med.* **2003**, *349*, 1731−1737.
(6) (a) Winder, C.; Carmichael, N. G.; Lewis, P. D. *Trends Neurosci.* **1982**, *5*, 207−209. (b) Araki, S.; Sato, H.; Yokoyama, K.; Murata, K. *Am. J. Ind. Med.* **2000**, *37*, 193−204. (c) Cory-Slechta, D. A. *Adv. Behav. Pharmacol.* **1984**, *4*, 211−255.
(7) Lin-Fu, J. S. Lead Poisoning, A Century of Discovery and Rediscovery. In *Human Lead Exposure*; Needleman, H. L., Ed.; Lewis Publishing: Boca Raton, FL, 1992.
(8) (a) McClure, D. S. *J. Chem. Phys.* **1952**, *20*, 682−686. (b) Varnes, A. W.; Dodson, R. B.; Whery, E. L. *J. Am. Chem. Soc.* **1972**, *94*, 946−950. (c) Bag, B.; Bharadwaj, P. K. *Inorg. Chem.* **2004**, *43*, 4626−2630.
(9) (a) Métivier, R.; Leray, I.; Valeur, B. *Chem.—Eur. J.* **2004**, *10*, 4480−4490. (b) Moon, S.-Y.; Youn, N. J.; Park, S. M.; Chang, S.-K. *J. Org. Chem.* **2005**, *70*, 2394−2397. (c) Park, S. M.; Kim, M. H.; Choe, J.-I.; No, K. T.; Chang, S.-K. *J. Org. Chem.* **2007**, *72*, 3550−3553. (d) Nolan, E. M.; Lippard, S. J. *Chem. Rev.* **2008**, *108*, 3443−3480. (e) Kim, Y.-H.; Youk, J. S.; Moon, S. Y.; Choe, J.-I.; Chang, S.-K. *Chem. Lett.* **2004**, *33*, 702−703. (f) Descalzo, A. B.; Martínez-Mánez, R.; Radeglia, R.; Rurack, K.; Soto, J. *J. Am. Chem. Soc.* **2003**, *125*, 3418−3419.
(10) (a) Kealy, T. J.; Pauson, P. L. *Nature* **1951**, *168*, 1039−1040. (b) Martin, N.; Sanchez, L.; Illescas, B.; Prez, I. *Chem. Rev.* **1998**, *98*, 2527−2548. (c) Beer, P. D. *Acc. Chem. Res.* **1998**, *31*, 71−80. (d) Bayly, S. R.; Beer, P. D.; Chen, G. Z. *Ferrocenes* **2008**, 281−318. (e) Kinbara, K.; Aida, K. *Chem. Rev.* **2005**, *105*, 1377−1400. (f) Miller, S. A.; Tebboth, A. J.; Tremaine, J. F. *J. Chem. Soc.* **1952**, 632−635. (g) Togni, A., Hayashi, T., Eds. *Homogenous Catalysts. Organic Synthesis, Material Science*; VCH: Weinheim, Germany, 1995.
(11) (a) Hayashi, T., Togni, A., Eds. *Ferrocenes*; VCH: Weinheim, Germany, 1995. (b) Dai, L.-X.; Tu, T.; You, S.-L.; Deng, W.-P.; Hou, X.-L. *Acc. Chem. Res.* **2003**, *36*, 659−667. (c) Sawamura, M.; Ito, Y. *Chem. Rev.* **1992**, *92*, 857−871. (d) Colacot, T. J. *Chem. Rev.* **2003**, *103*, 3101−3118. (e) Arráyas, R. G.; Adrio, J.; Carretero, J. C. *Angew. Chem., Int. Ed.* **2006**, *45*, 7674−7715. (f) Atkinson, R. C. J.; Gibson, V. C.; Long, N. J. *Chem. Soc. Rev.* **2004**, *33*, 313−328. (g) Soai, K.; Shibata, T.; Morioka, H.; Choji, K. *Nature* **1995**, *378*, 767−768. (h) Sato, I.; Urabe, H.; Ishiguro, S.; Shibata, T.; Soai, K. *Angew. Chem., Int. Ed.* **2003**, *42*, 315−317. (i) Soai, K.; Shibata, T.; Sato, I. *Acc. Chem. Res.* **2000**, *33*, 382−390. (j) Soai, K.; Sato, I.; Shibata, T. In *Methodologies in Asymmetric Catalysis*; Malhotra, S. V., Ed.; American Chemical Society: Washington, DC, 2004; pp 85−102. (k) Todd, M. H. *Chem. Soc. Rev.* **2002**, *31*, 211−222. (l) Blackmond, D. G. *Proc. Natl. Acad. Sci. U.S.A.* **2004**, *101*, 5732−5736. (m) Moriuchi, T.; Hirao, T. *Top. Organomet. Chem.* **2006**, *17*, 143−175.
(12) Hillard, E.; Vessieres, A.; Bideau, F. L.; Plazuk, D.; Spera, D.; Huche, M.; Jaouen, G. *ChemMedChem.* **2006**, *1*, 551−559, and references cited therein.
(13) (a) Tsuji, J. *Palladium reagents and catalysts*; Wiley-VCH: New York, 1999. (b) Beccalli, E. M.; Broggini, G.; Martinelli, M.; Sottocornola, S. *Chem. Rev.* **2007**, *107*, 5318−5365.
(14) (a) Plesske, K. *Angew. Chem., Int. Ed.* **1962**, *1*, 312−327. (b) Plesske, K. *Angew. Chem., Int. Ed.* **1962**, *1*, 394−399.
(15) (a) Tebben, L.; Bussmann, K.; Hegemann, M.; Kehr, G.; Fröhlich, R.; Erker, G. *Organometallics* **2008**, *27*, 4269−4272. (b) Van Staveren, D. R.; Metzler-Nolte, N. *Chem. Rev.* **2004**, *104*, 5931−5985. (c) Han, Y.; Cheng, K.; Simon, K. A.; Lan, Y.; Sejwal, P.; Luk, Y. Y. *J. Am. Chem. Soc.* **2006**, *128*, 13913−13920.
(16) (a) Shen, Q.; Ogata, T.; Hartwig, J. F. *J. Am. Chem. Soc.* **2008**, *130*, 6586−6596. (b) Hattori, T.; Sakamoto, J.; Hayashizaka, N.; Miyano, S. *Synthesis* **1994**, 199−202. (c) Semmelhack, M. F.; Rhee, H. *Tetrahedron Lett.* **1993**, *34*, 1395−1398. (d) Paine, A. J. *J. Am. Chem. Soc.* **1987**, *109*, 1496−1502. (e) Ten Hoeve, W.; Kruse, C. G.; Luteyn, J. M.; Thiecke, J. R. G.; Wynberg, H. *J. Org. Chem.* **1993**, *58*, 5101−5106.
(17) (a) Molina, P.; Tarraga, A.; Caballero, A. *Eur. J. Inorg. Chem.* **2008**, 3401−3417. (b) Caballero, A.; García, R.; Espinosa, A.; Tárraga, A.; Molina, P. *J. Org. Chem.* **2007**, *72*, 1161−1173. (c) Joseph, R.; Ramanujam, B.; Acharya, A.; Khutia, A.; Rao, C. P. *J. Org. Chem.* **2008**, *73*, 5745−5758.
(18) Perrin, D. D.; Armango, W. L. F.; Perrin, D. R. *Purification of Laboratory Chemicals*; Pergamon: Oxford, U.K., 1986.
(19) Sheldrick, G. M. *SHELXL-97, Program for X-ray Crystal Structure Refinement*; Göttingen University: Göttingen, Germany, 1997. (b) Sheldrick, G. M. *SHELXS-97, Program for X-ray Crystal Structure Solution*; Göttingen University: Göttingen, Germany, 1997.
(20) (a) Spek, A. L. *PLATON, A Multipurpose Crystallographic Tools*; Utrecht University: Utrecht, The Netherlands, 2000. (b) Spek, A. L. *Acta Crystallogr., Sect. A* **1990**, *46*, C31.
(21) (a) Bartolottiand, L. J.; Fluchick, K. In *Reviews in Computational Chemistry*; Lipkowitz, K. B., Boyd, D., Ed.; VCH: New York, 1996; Vol. 7, pp 187−216. (b) Becke, A. D. *J. Chem. Phys.* **1993**, *98*, 5648−5652. (c) Lee, C. T.; Yang, W. T.; Parr, R. G. *Phys. Rev. B* **1988**, *37*, 785−789. (d) Hay, P.; Wadt, W. R. *J. Chem. Phys.* **1985**, *82*, 270−283. (e) Wadt, W. R.; Hay, P. *J. Chem. Phys.* **1985**, *82*, 284−298. (f) Hay, P.; Wadt, W. R. *J. Chem. Phys.* **1985**, *82*, 299−310.
(22) Frisch, M. J.; Trucks, G. W.; Schlegel, H. B.; Scuseria, G. E.; Robb, M. A.; Cheeseman, J. R.; Montgomery, J. A., Jr.; Vreven, T.; Kudin, K. N.; Burant, J. C.; Millam, J. M.; Iyengar, S. S.; Tomasi, J.; Barone, V.; Mennucci, B.; Cossi, M.; Scalmani, G.; Rega, N.; Petersson, G. A.; Nakatsuji, H.; Hada, M.; Ehara, M.; Toyota, K.; Fukuda, R.; Hasegawa, J.; Ishida, M.; Nakajima, T.; Honda, Y.; Kitao, O.; Nakai, H.; Klene, M.; Li, X.; Knox, J. E.; Hratchian, H. P.; Cross, J. B.; Bakken, V.; Adamo, C.; Jaramillo, J.; Gomperts, R.; Stratmann, R. E.; Yazyev, O.; Austin, A. J.; Cammi, R.; Pomelli, C.; Ochterski, J. W.; Ayala, P. Y.; Morokuma, K.; Voth, G. A.; Salvador, P.; Dannenberg, J. J.; Zakrzewski, V. G.; Dapprich, S.; Daniels, A. D.; Strain, M. C.; Farkas, O.; Malick, D. K.; Rabuck, A. D.; Raghavachari, K.; Foresman, J. B.; Ortiz, J. V.; Cui, Q.; Baboul, A. G.; Clifford, S.; Cioslowski, J.; Stefanov, B. B.; Liu, G.; Liashenko, A.; Piskorz, P.; Komaromi, I.; Martin, R. L.; Fox, D. J.; Keith, T.; Al-Laham, M. A.; Peng, C. Y.; Nanayakkara, A.; Challacombe, M.; Gill, P. M. W.; Johnson, B.; Chen, W.; Wong, M. W.; Gonzalez, C.; Pople, J. A. *Gaussian 03*, revision B.03; Gaussian, Inc.: Wallingford, CT, 2004.
(23) (a) Troshin, P. A.; Troyanov, S. I.; Boiko, G. N.; Lyubovskaya, R. N.; Lapshin, A. N.; Goldshleger, N. F. *Fullerenes, Nanotubes, Carbon Nanostruct.* **2004**, *12*, 413−419. (b) Hampe, D.; Günther, W.; Görls, H.; Anders, E. *Eur. J. Org. Chem.* **2004**, 4357−4372. (c) Crugeiras, J.; Rios, A.; Amyes, T. L.; Richard, J. P. *Org. Biomol. Chem.* **2005**, *3*, 2145−2149.
(24) (a) Desiraju, G. R. *Acc. Chem. Res.* **1996**, *29*, 441−449. (b) Desiraju, G. R. *Angew. Chem., Int. Ed.* **1995**, *34*, 2311−2327.
(25) (a) Geoffroy, G. L.; Wrighton, M. S. *Organometallic Photochemistry*; Academic Press: New York, 1979. (b) Sohn, Y. S.;

Hendrickson, D. N.; Gray, H. B. *J. Am. Chem. Soc.* **1971**, *93*, 3603−3612. (c) Delavaux-Nicot, B.; Maynadiè, J.; Lavabre, D.; Fery-Forgues, S. *Inorg. Chem.* **2006**, *45*, 5691−5702. (d) Basurto, S.; Riant, O.; Moreno, D.; Rojo, J.; Torroba, T. *J. Org. Chem.* **2007**, *72*, 4673−4688. (e) Willener, Y.; Joly, K. M.; Moody, C. J.; Tucker, J. H. R. *J. Org. Chem.* **2008**, *73*, 1225−1233.

(26) (a) Yub, Y.; Lin, L.-R.; Yang, K.-B.; Zhong, X.; Huang, R.-B.; Zheng, L.-S. *Talanta* **2006**, *69*, 103−106. (b) Zhu, M.; Yuan, M.; Liu, X.; Xu, J.; Lv, J.; Huang, C.; Liu, H.; Li, Y.; Wang, S.; Zhu, D. *Org. Lett.* **2008**, *10*, 1481−1484. (c) Elanchezhian, S. V.; Kandaswamy, M. *Inorg. Chem. Commun.* **2010**, *13*, 1109−1113. (d) Zapata, F.; Caballero, A.; Espinosa, A.; Tárraga, A.; Molina, P. *Inorg. Chem.* **2009**, *48*, 11566−11575. (e) Caballero, A.; Espinosa, A.; Tárraga, A.; Molina, P. *J. Org. Chem.* **2007**, *72*, 6924−6937. (f) Caballero, A.; Espinosa, A.; Tárraga, A.; Molina, P. *J. Org. Chem.* **2008**, *73*, 5489−5497.

(27) (a) Kimura, J.; Yamada, H.; Yajima, T.; Fukushima, T. *J. Lumin.* **2009**, *129*, 1362−1365. (b) Godde, F.; Toulmé, J.-J.; Moreau, S. *Nucleic Acids Res.* **2000**, *28*, 2977−2985. (c) Biavardi, E.; Battistini, G.; Montalti, M.; Yebeutchou, R. M.; Prodi, L.; Dalcanale, E. *Chem. Commun.* **2008**, 1638−1640. (d) Shirdel, J.; Penzkofer, A.; Shen, Z.; Procházka, R.; Daub. *J. Chem. Phys.* **2007**, *337*, 99−109.

(28) (a) Hirano, K.; Oderaotoshi, Y.; Minataka, S.; Komatsu, M. *Chem. Lett.* **2001**, 1262−1263. (b) Vivas-Mejía, P.; Rodríguez-Cabán, J. L.; Díaz-Velázquez, M.; Hernández-Pérez, M. G.; Cox, O.; Gonzalez, F. A. *Mol. Cell. Biochem.* **1997**, *177*, 69−77.

(29) (a) Bazzicalupi, C.; Bencini, A.; Bianchi, A.; Giorgi, C.; Fusi, V.; Valtancoli, B.; Bernardo, M. A.; Pina, F. *Inorg. Chem.* **1999**, *38*, 3806−3813. (b) Rurack, K. *Spectrochim. Acta A* **2001**, *57*, 2161−2195. (c) Wang, F.; Schwabacher, A. W. *J. Org. Chem.* **1999**, *64*, 8922−8928. (d) Melnick, J. G.; Yurkerwich, K.; Parkin, G. *Inorg. Chem.* **2009**, *48*, 6763. (e) Torrado, A.; Walkup, G. K.; Imperiali, B. *J. Am. Chem. Soc.* **1998**, *120*, 609−610. (f) Zapata, F.; Caballero, A.; Espinosa, A.; Tárraga, A.; Molina, P. *Dalton Trans.* **2010**, *39*, 5429−5431. (g) Williams, N. J.; Gan, W.; Reibenspies, J. H.; Hancock, R. D. *Inorg. Chem.* **2009**, *48*, 1407−1415. (h) Xue, L.; Liu, Q.; Jiang, H. *Org. Lett.* **2009**, *11*, 3454−3457.

(30) Zapata, F.; Caballero, A.; Espinosa, A.; Tárraga, A.; Molina, P. *J. Org. Chem.* **2009**, *74*, 4787−4796.

(31) (a) Connors, K. A. *Binding Constants*; Wiley: New York, 1987. (b) Mashraqui, S. H.; Khan, T.; Sundaram, S.; Betkar, R.; Chandiramani, M. *Tetrahedron Lett.* **2007**, *48*, 8487−8490.

(32) (a) Goldstein, G. W. *Neurotoxicology* **1993**, *14*, 97−102. (b) Simons, T. J. B. *Neurotoxicology* **1993**, *14*, 77−86. (c) Goyer, R. A. *Environ. Health Perspect.* **1990**, *86*, 177−182.

(33) Ahamed, B. N.; Arunachalam, M.; Ghosh, P. *Inorg. Chem.* **2010**, *49*, 4447−4457.

(34) Carr, J. D.; Coles, S. J.; Hassan, W. W.; Hursthouse, M. B.; Malik, K. M. A.; Tucker, J. H. R. *J. Chem. Soc., Dalton Trans.* **1999**, 57−62.

(35) Caballero, A.; Lloveras, V.; Tárraga, A.; Espinosa, A.; Velasco, M. D.; Vidal-Gancedo, J.; Rovira, C.; Wurst, K.; Molina, P.; Veciana, J. *Angew. Chem., Int. Ed.* **2005**, *44*, 1977−1981.